Nonstationarity in the NAO–Gulf Stream SST Front Interaction

LUCA FAMOOSS PAOLINI,[a,b,c] NOUR-EDDINE OMRANI,[d] ALESSIO BELLUCCI,[e] PANOS J. ATHANASIADIS,[a] PAOLO RUGGIERI,[a,c] CASEY R. PATRIZIO,[a] AND NOEL KEENLYSIDE[d,f]

[a] *Fondazione Centro Euro-Mediterraneo sui Cambiamenti Climatici, Bologna, Italy*
[b] *Department of Environmental Science, Informatics and Statistics, Ca' Foscari University, Venice, Italy*
[c] *Department of Physics and Astronomy, University of Bologna, Bologna, Italy*
[d] *Geophysical Institute, University of Bergen and Bjerkenes Centre for Climate Research, Bergen, Norway*
[e] *Consiglio Nazionale delle Ricerche, Istituto di Scienze dell'Atmosfera e del Clima, Bologna, Italy*
[f] *Nansen Environmental and Remote Sensing Center, Bergen, Norway*

(Manuscript received 10 August 2023, in final form 5 December 2023, accepted 6 December 2023)

ABSTRACT: The interaction between the North Atlantic Oscillation (NAO) and the latitudinal shifts of the Gulf Stream sea surface temperature front (GSF) has been the subject of extensive investigations. There are indications of nonstationarity in this interaction, but differences in the methodologies used in previous studies make it difficult to draw consistent conclusions. Furthermore, there is a lack of consensus on the key mechanisms underlying the response of the GSF to the NAO. This study assesses the possible nonstationarity in the NAO–GSF interaction and the mechanisms underlying this interaction during 1950–2020, using reanalysis data. Results show that the NAO and GSF indices covary on the decadal time scale but only during 1972–2018. A secondary peak in the NAO–GSF covariability emerges on multiannual time scales but only during 2005–15. The nonstationarity in the decadal NAO–GSF covariability is also manifested in variations in their lead–lag relationship. Indeed, the NAO tends to lead the GSF shifts by 3 years during 1972–90 and by 2 years during 1990–2018. The response of the GSF to the NAO at the decadal time scale can be interpreted as the joint effect of the fast response of wind-driven oceanic circulation, the response of deep oceanic circulation, and the propagation of Rossby waves. However, there is evidence of Rossby wave propagation only during 1972–90. Here it is suggested that the nonstationarity of Rossby wave propagation caused the time lag between the NAO and the GSF shifts on the decadal time scale to differ between the two time periods.

KEYWORDS: North Atlantic Ocean; Rossby waves; Boundary currents; Air–sea interaction; Decadal variability; North Atlantic Oscillation

1. Introduction

Recent studies have shown that the extratropical atmospheric circulation in the Northern Hemisphere is significantly influenced by the oceanic front associated with the current known as the Gulf Stream (GS) (e.g., O'Reilly et al. 2016; Joyce et al. 2019). Specifically, the presence of the GS sea surface temperature (SST) front (GSF) has been shown to shape the climatological structure of the North Atlantic storm-track and eddy-driven jet (Brayshaw et al. 2011; O'Reilly et al. 2016; Omrani et al. 2019). Furthermore, the meridional displacements of the GSF have been shown to affect the North Atlantic tropospheric variability, with atmospheric circulation anomalies extending up to the Eurasian continent (Joyce et al. 2009; Nakamura and Yamane 2009; Kwon and Joyce 2013; Sato et al. 2014; Famooss Paolini et al. 2022). Therefore, studying the drivers of the GSF variability is important for understanding the associated coupled (ocean–atmosphere) variability and predictability.

The GSF latitudinal position has been linked to the Atlantic meridional overturning circulation (AMOC; e.g., de Coëtlogon et al. 2006; Sanchez-Franks and Zhang 2015) and to different climate modes of variability, such as the Atlantic meridional mode (Hameed et al. 2018; Wolfe et al. 2019), the Atlantic multidecadal oscillation (Nigam et al. 2018), El Niño–Southern Oscillation (ENSO; e.g., Taylor et al. 1998; Sanchez-Franks et al. 2016), and the North Atlantic Oscillation (NAO; e.g., Taylor and Stephens 1998; Joyce et al. 2000; Frankignoul et al. 2001; Hameed and Piontkovski 2004; Kwon et al. 2010; Pérez-Hernández and Joyce 2014; Sanchez-Franks et al. 2016; Wolfe et al. 2019). In this context, particular attention has been directed toward the NAO, which is the dominant mode of variability of the surface atmospheric circulation in the North Atlantic region (Hurrell 1995).

The NAO can affect the GSF latitudinal position through anomalous wind stress over the North Atlantic, by directly changing the wind-driven oceanic circulation and by exciting westward propagating Rossby waves (Gangopadhyay et al. 2016). For example, the positive phase of the NAO is associated with anomalous northward Ekman transport over the GS region (Visbeck et al. 2003) and a northward shift of the zero wind stress curl line. The resulting wind-driven oceanic circulation anomalies are generally largest at the confluence of the subpolar and subtropical gyres (Marshall et al. 2001;

Denotes content that is immediately available upon publication as open access.

Supplemental information related to this paper is available at the Journals Online website: https://doi.org/10.1175/JCLI-D-23-0476.s1.

Corresponding author: Luca Famooss Paolini, luca.famoosspaolini@unibo.it

DOI: 10.1175/JCLI-D-23-0476.1

Reintges et al. 2017) and may thus influence the position of the GSF. Indeed, previous studies have shown that a positive NAO results in a northward displacement of the GSF, which can lag the NAO forcing by less than one month up to 2–3 years (Taylor and Stephens 1998; Joyce et al. 2000; Frankignoul et al. 2001; Taylor and Gangopadhyay 2001; Joyce et al. 2019; Watelet et al. 2020). Similarly, a negative NAO results in a southward displacement of the GSF with similar time lags. The time lags have been related to the time that fast barotropic and slow baroclinic planetary waves require to travel from the eastern to western North Atlantic (Veronis 1973; Gangopadhyay et al. 1992; Marshall et al. 2001; Bellucci and Richards 2006). As an example, in a numerical study, Sasaki and Schneider (2011) have shown that the NAO can affect the GS position through westward propagating sea level height anomalies generated by anomalous Ekman convergence in the central North Atlantic, which reach the GS area after about 2 years. Consistently, in another numerical study, de Coëtlogon et al. (2006) have shown evidence of NAO-forced baroclinic Rossby wave propagation in the southern part of the subpolar gyre, which affects the GS path and transport after about 2 years. However, the impact of Rossby wave propagation on the GSF position remains unclear from previous studies. Indeed, several studies have documented the characteristics of oceanic Rossby waves in North Atlantic propagating with phase velocities in the 0.93–4.17 cm s^{-1} range (Cipollini et al. 1997, 2001; Osychny and Cornillon 2004; de Coëtlogon et al. 2006; Watelet et al. 2020; Årthun et al. 2021). These phase velocities imply a time lag between the NAO and the GSF shifts that is greater than observed, even for waves that are generated in the mid-Atlantic (Frankignoul et al. 2001; Wolfe et al. 2019).

Furthermore, the NAO can indirectly affect the GSF position through buoyancy fluxes in the Labrador Sea (Joyce et al. 2000; Peña-Molino and Joyce 2008; Watelet et al. 2020). The NAO is associated with anomalous surface heat fluxes over the subpolar gyre, which can impact deep convection and thus the export of Labrador Sea Water via the deep western boundary current (DWBC). Once the deep water is formed, it is partly recirculated within the Labrador Sea and along the North Atlantic Current and partly transported southward, flowing along the Slope Sea (Stommel 1958; Csanady and Hamilton 1988; Bower et al. 2009, 2011). Here the Slope Sea refers to the region between the GS and the eastern continental shelf of North America, from Cape Hatteras to the Grand Banks. Zhang and Vallis (2007) have shown that bottom vortex stretching of the DWBC transport is able to affect the GS latitudinal position by changing the intensity of the northern recirculation gyre (NRG), a barotropic cyclonic circulation north of the GS (Hogg 1992). The stronger (weaker) the DWBC transport close to the Grand Banks, the stronger (weaker) the NRG and the more southward (northward) the GS. The effect of the DWBC transport on the GS latitudinal position has been suggested to be particularly relevant on the decadal and multidecadal time scales (Zhang and Vallis 2006). Indeed, the DWBC feeds the deeper branch of the AMOC, which has been shown to be affected by the NAO on these time scales (Bellucci and Richards 2006; Bellucci et al. 2008; Reintges et al. 2017; Omrani et al. 2022).

In the context of the NAO forcing changes in the GS latitudinal position through its effect on the DWBC transport, Joyce et al. (2000) have speculated on the existence of a self-sustained decadal NAO–GS coupled oscillation using a simple oceanic model. In this oscillation, a positive NAO enhances the southward transport of Labrador Sea Water in the DWBC. The anomalies propagate southward along the eastern continental shelf of North America and reach the GS area after some years. This propagation time lag depends on the values of model parameters. The enhanced transport of Labrador Sea Water in response to the positive NAO acts to move the GS separation point close to Cape Hatteras southward (Pickart and Smethie 1993; Spall 1996). Consequently, negative SST anomalies are established along the GS, modifying the atmospheric transient eddy activity and influencing the NAO phase. Finally, the reversal of the NAO phase changes the buoyancy forcing in the Labrador Sea and the cycle starts again with the opposite sign. In agreement with this mechanism acting on the decadal time scale, Peña-Molino et al. (2011) have shown in an observational study that anomalies in Labrador Sea Water require approximately 4–9 years to propagate from the Labrador Sea to the north–east of Cape Hatteras. Similarly, Molinari et al. (1998) have estimated a transit time from the Labrador Sea to 26.5°N of about 10 years. Using chlorofluorocarbon and hydrographic data, Smethie (1993) has inferred an even longer transit time (about 18 years). However, it is unclear whether such a decadal NAO–GS oscillation operates in reality since observational support is lacking.

Some studies have shown that a significant part of the Labrador Sea Water is not exported from the Labrador Sea via the DWBC but instead follows other southward-oriented pathways (Rossby 1999; Rossby and Benway 2000; Rossby et al. 2005; Bower et al. 2009, 2011). In agreement with these studies, analyzing observational and reanalysis data, Hameed and Piontkovski (2004) and Sanchez-Franks et al. (2016) have shown that the pressure and the longitude of the Icelandic low (i.e., one NAO center of action) are good predictors for the GS latitudinal position on interannual time scale. In particular, enhanced (reduced) and westward (eastward) shifted Icelandic low intensifies (reduces) the transport of the surface Labrador Current, thus reducing (enhancing) the cold water sources along the Slope Water (i.e., the upper 500 m of the water column in the Slope Sea) and shifting northward (southward) the GS (Peterson et al. 2017; Holliday et al. 2020; New et al. 2021). The highest predictive skill has been obtained when the enhanced and westward shifted Icelandic low leads the GSF latitudinal position by 2–3 years. However, other studies have estimated that the temperature and salinity anomalies in the Slope Water would take about 4–18 months to travel from the Newfoundland to the GS separation point (Rossby et al. 2005; Peña-Molino and Joyce 2008; Peterson et al. 2017; New et al. 2021). This suggests a shorter time lag between the NAO forcing and the GS shifts relative to the ones proposed by Hameed and Piontkovski (2004) and Sanchez-Franks et al. (2016).

Hameed and Piontkovski (2004) have also shown that the effect of the Azores high (i.e., the other NAO center of action) on the GS latitudinal position is insignificant during 1965–2000. For this reason, they have concluded that the

influence of the NAO on the GS latitudinal position through changing the southward flow of Labrador Sea Water is dominant in comparison with its influence through Rossby waves excited in the extratropical North Atlantic. However, they have analyzed the time period 1965–2000 as a whole. On the other hand, Sasaki and Schneider (2011), looking at the nonstationarity of time series in an oceanic model forced with observed atmospheric fluxes, have provided evidence of wave propagation during 1965–85 that affects the GS path. The different methodological approach of these two studies suggest that the westward wave propagation is present during specific time periods and hence is suggestive of nonstationarity in the NAO–GSF interaction.

Previous studies have shown that a variety of mechanisms can contribute to the interaction between the NAO and the GSF, but the primary mechanisms behind the response of the GSF to the NAO in observations remain unclear. The lack of consensus is emphasized by a wide range of time lags between meridional displacements of the GSF and the NAO reported among prior studies, ranging between 0 and 4 years (Table 1). In this context, time lags between 0 and 2 years are most commonly reported (Fig. S1 in the online supplemental material). The discrepancies between studies may be linked to differences in the definition of the GS latitudinal position, which has been based both on surface (Taylor and Stephens 1998; Watelet et al. 2020) and subsurface data (Joyce et al. 2000; Hameed et al. 2018) and has adopted different space domains (Hameed et al. 2018). These discrepancies might also be linked to differences in the datasets (models, observations, and reanalyses) and methodological approaches. In particular, analyses that do not consider the nonstationarity of the mechanisms involved can miss capturing some of them (e.g., the wave propagation; Hameed and Piontkovski 2004; Sasaki and Schneider 2011). Last, the discrepancies might be linked to differences in the analyzed time period. In some cases, this could reflect disparities in the quality and coverage of observations, but this could also suggest that the NAO–GSF interaction is nonstationary in time (Frankignoul et al. 2001; Hameed and Piontkovski 2004; Sasaki and Schneider 2011; Lillibridge and Mariano 2013; Hameed et al. 2018). For example, using a revised index for the latitudinal position of the GS north wall, Hameed et al. (2018) showed that the NAO leads the GS shifts by 1 year in 1940–2014 and 0 year in 1961–2014, while no lag correlation was found in 2005–14.

To summarize, there is a lack of consensus on the key mechanisms underlying the response of the GSF to the NAO. There are also indications of nonstationarity in the NAO–GSF interaction. However, it is difficult to draw robust conclusions due to differences among methodologies used in prior studies, including differences in the time period of analysis and indices of GSF variability. The goal of this study is to assess the possible nonstationarity in the NAO–GSF interaction during the winter season and to help clarify the mechanisms underlying this interaction over the last few decades using the fifth major global reanalysis produced by ECMWF (ERA5) and Ocean Reanalysis System 5 (ORAS5) reanalysis data.

The paper is structured as follows. In section 2 the data and the methodological approach are described. In section 3 the spectral features of the NAO–GSF covariability and the mechanisms through which the NAO may be forcing the GSF latitudinal position at the decadal time scale are presented. In section 4 we discuss some aspects of the nonstationarity in the NAO–GSF relation and the associated mechanisms. In section 5 we summarize the main outcomes of the present work.

2. Data and methodological approach

a. Data

The interaction between the GSF and the NAO has been assessed in this study using ERA5 atmospheric reanalysis (Hersbach et al. 2020) and ORAS5 oceanic reanalysis (Zuo et al. 2019) data in the period 1950–2020 and 1958–2018, respectively. The ORAS5 reanalysis is forced by ERA-40 and ERA-Interim reanalysis during 1958–78 and 1979–2014, respectively. From 2015 onward, the ORAS5 reanalysis is forced by ECMWF/IFS operational analysis. These atmospheric products are consistent with ERA5 reanalysis in terms of representation of large-scale modes of atmospheric variability such as the NAO (not shown). Thus, using the more recent and accurate ERA5 reanalysis as a reference for the atmospheric state instead of the other ECMWF products does not affect the NAO–GSF interaction and the interpretation of results presented here.

The GSF has been defined as the line of maximum SST gradient, following the procedure described in Famooss Paolini et al. (2022). Specifically, the SST gradient magnitude has been calculated for SST data averaged in the winter season (December–February) and smoothed with a 2D spatial Gaussian–Kernel filter applied to a 7×7 gridpoint box, with standard deviation equal to 2. The winter season has been selected as the season in which the ocean–atmosphere interaction is the most intense (Kallberg et al. 2005). The spatial smoothing has been applied to remove isolated points of strong SST gradient not representative of the GSF. Then, the latitude of the GSF has been calculated as the average over the 50°–68°W longitudinal range. The GSF latitude (i.e., the GSF index) has been computed using ERA5 data. SST data are also provided in ORAS5 reanalysis; however, this reanalysis exhibits SST biases in the GS region (Zuo et al. 2019), which may affect the representation of the GSF latitudinal position.

Similarly to the approach followed by Hurrell et al. (2003), the NAO has been defined as the leading principal component of winter mean sea level pressure (SLP) over the North Atlantic sector (0°–80°N, 90°W–40°E). Prior to the index calculation, SLP data have been scaled by a factor $[\cos(\text{latitude})]^{1/2}$ so that different grid cells contribute to the variance of the field proportionally to the area they represent.

b. Methods

1) Cross-wavelet analysis

To assess the NAO–GSF interaction and its spectral features, a cross-wavelet analysis has been applied (Torrence

TABLE 1. Time lags between the GS meridional displacements and the NAO-related forcing. Columns detail the index to define the GS latitudinal position, the index to define the NAO-related forcing, the typology of the analyzed dataset, the period over which the data have been averaged, the analyzed time period, the time lag, and the reference. Only the time lags for which the correlation between the GS index and the NAO-related index is statistically significant at 90% and 95% confidence levels are shown in the table. The following acronyms are used in the table: GS is Gulf Stream, GSNW is Gulf Stream North Wall, GSI is Gulf Stream index, eGSI is extended GSI, GST is Gulf Stream temperature, SSH is sea surface height, NAO is North Atlantic Oscillation, IL is Icelandic low, and AH is Azores high. Refer to the respective references for more details.

GS index	NAO-related index	Data	Time mean	Time period	Time lag	Reference
GSNW	NAO	Observations	Dec–Mar	1966–96	2 years	Taylor and Stephens (1998)
GSI	NAO	Observations	Jan–Mar	1954–89	0–1 year	Joyce et al. (2000)
Surface salinity data	NAO	Observations	Dec–Feb	1978–98	1.5 years	Rossby and Benway (2000)
GSI	NAO	Observations	Monthly Annual	1955–98	12–18 months 0–2 years	Frankignoul et al. (2001) Frankignoul et al. (2001)
GSNW	IL pressure IL lat IL lon AH pressure AH lat AH lon	Observations	Dec–Feb	1966–2000	1–3 years 1–2 years 3–4 years 0–2 years No correlation 2 years	Hameed and Piontkovski (2004)
GSNW	NAO	Observations (ocean); reanalysis (atmosphere)	Annual	1954–98	0–3 years	de Coëtlogon et al. (2006)
GST index (similar to GSNW)		Model (ocean); reanalysis (atmosphere)		1948–2000	0–2 years	de Coëtlogon et al. (2006)
GSNW	NAO	Observations	Dec–Mar	1980–99	1 year	Chaudhuri et al. (2009)
SSH data	NAO	Model	Dec–Mar	1960–2003	2 years	Sasaki and Schneider (2011)
GSI	Synoptic transient eddy heat flux	Observations (ocean); reanalysis (atmosphere)	Jan–Mar	1979–2009	2 years	Kwon and Joyce (2013)
SSH data	NAO	Observations	Monthly	1992–2011	6 months	Lillibridge and Mariano (2013)
16-point GS index (based on SSH data)	NAO	Model	Dec–Mar	1960–2003	2 years	Pérez-Hernández and Joyce (2014)
GSNW	IL pressure IL longitude NAO	Observations (ocean); reanalysis (atmosphere)	Annual	1966–2014	0–2 years 3–4 years 0–2 years	Sanchez-Franks et al. (2016)
GSNW-revised	NAO	Observations (ocean); reanalysis (atmosphere)	Annual	1940–2014	1 year	Watelet et al. (2017)
eGSI-0m	NAO	Observations (ocean); reanalysis (atmosphere)	Annual	1961–2015 2005–15	0 year No correlation	Hameed et al. (2018)
eGSI-200m (comparable to GSI)				1961–2015 2005–15	0–1 year No correlation	
GSNW				1966–2014 2005–2014	0–2 years No correlation	
wGSNW			Annual Dec–Feb Annual	1940–2014 1940–2014 1961–2014 2005–14	1 year 0 year 0 year No correlation	

TABLE 1. (*Continued*)

GS index	NAO-related index	Data	Time mean	Time period	Time lag	Reference
eGSI-0m	IL pressure	Observations (ocean); reanalysis (atmosphere)	Dec–Feb	1961–2015	0–2 years	Wolfe et al. (2019)
	IL lat				0–1 year	
	IL lon				1 year	
	AH pressure				0–2 years	
	AH lat				No correlation	
	AH lon				No correlation	

and Compo 1998; Grinsted et al. 2004). The NAO and GSF time series have been linearly detrended and standardized before performing the cross-wavelet analysis. The cross-wavelet analysis is a mathematical tool developed for the analysis of the relationship between two time series in the time–frequency phase space (Hudgins et al. 1993). This tool allows us to study how the cospectral features evolve in time, which is useful in assessing also the nonstationarity of the relationship between two variables. In particular, the relationship between two time series is assessed through the cross-wavelet power spectrum, which can indicate domains in the time–frequency space where the two time series share high power (Torrence and Compo 1998). However, peaks in the cross-wavelet power spectrum can appear in a given frequency range when two time series are independent and only one of them features significantly high power in this range (Maraun and Kurths 2004). For this reason, another common measure for the relationship between two time series is the squared wavelet coherence (i.e., the cross-wavelet power spectrum normalized by the wavelet power spectrum of both time series). This coefficient provides a good estimate of the correlation between two time series in the time–frequency space (Grinsted et al. 2004), but spurious peaks can occur in areas with low wavelet power. Finally, the time lag between two time series is estimated through the phase of the cross-wavelet power spectrum, defined as the arctan of the ratio between its real and imaginary part.

The Morlet function has been adopted as the wavelet basis function, with nondimensional frequency ω_0 equal to 6 to satisfy the admissibility condition (Farge 1992). The statistical significance of the NAO–GSF cross-wavelet power spectrum has been assessed with the procedure detailed in Torrence and Compo (1998; refer to their section 6c), assuming the white- and red-noise spectra as background spectra for the NAO and the GSF, respectively. The statistical significance of the squared wavelet coherence has been assessed through a Monte Carlo test, performing 300 simulations. In both cases, the 90% confidence level has been used. The phase relationship between the NAO and the GSF has been considered statistically significant when the squared wavelet coherence exceeds the 90% confidence level (Kohyama et al. 2021).

The spectral features of both time series have been further assessed through the wavelet transform, in order to verify whether peaks in the NAO–GSF cross-wavelet power spectrum and squared wavelet coherence are associated with peaks in the NAO and GSF wavelet power spectra. Results from the wavelet analysis applied to the single time series are also presented here as global wavelet power spectra (i.e., wavelet power spectra averaged along the time dimension). The global wavelet power spectrum provides a consistent estimate of the power spectrum of a time series (Percival 1995) and it closely approximates the Fourier spectrum (Hudgins et al. 1993; Torrence and Compo 1998). The NAO and GSF power spectra have been assessed also with the fast Fourier transform to make possible the comparison between the global wavelet and Fourier power spectra. The statistical significance of global wavelet power spectra has been assessed following the procedure described in Torrence and Compo (1998; refer to their section 5a), assuming the white- and red-noise spectra as background spectrum for the NAO and the GSF respectively.

2) LANCZOS BANDPASS FILTER

As described later in section 3, the cross-wavelet analysis shows that the NAO–GSF covariability is particularly prominent at a period range of 6–11 years. To assess the mechanisms through which the NAO may be forcing the GSF latitudinal position on the decadal time scale, data have been temporally filtered using a Lanczos bandpass filter with a period of 6–11 years and a window of 12 coefficients (Duchon 1979). The number of coefficients has been subjectively chosen to balance the filtering with the number of data lost at the beginning and end of the time series. However, the general features of the lead–lag relationships between time series discussed in later sections are rather insensitive to the number of coefficients ranging from 5 to 25.

It is here important to specify that the use of the bandpass filter induces a periodicity of about 8–9 years in the data. This aspect must be carefully taken into account during the interpretation of results described in the next sections, such as the causal link between the NAO forcing and the mechanisms through which the NAO can force the GSF latitudinal position.

3) INDICES

The NAO can affect the GSF latitudinal position through anomalous wind stress over the North Atlantic, influencing the wind-driven oceanic circulation and exciting Rossby waves (Gangopadhyay et al. 1992; Taylor and Stephens 1998; Joyce et al. 2000; Marshall et al. 2001; Taylor and Gangopadhyay 2001; Gangopadhyay et al. 2016), as well as through buoyancy forcing over the Labrador Sea, affecting the formation of Labrador Sea Water (Hameed and Piontkovski 2004; Zhang and Vallis 2007; Peña-Molino and Joyce 2008; Sanchez-Franks et al. 2016). The

following approaches have been adopted to assess the mechanisms through which the NAO drives the GSF latitudinal position.

Since the NAO affects the meridional Ekman transport over the GSF area (Visbeck et al. 2003; Deser et al. 2010), the response of the wind-driven oceanic circulation to the NAO has been assessed by averaging the winter meridional Ekman transport over the 50°–68°W longitudinal range (where the GSF is defined) and the 35°–40°N latitudinal range. A positive (negative) Ekman index indicates an anomalous northward (southward) Ekman transport over the GS region.

The presence of Rossby wave–like patterns in the extratropical North Atlantic has been assessed through the Hovmöller diagram (Hovmöller 1949) of the bandpass-filtered SST and sea surface height (SSH) anomalies averaged in the 35°–38°N latitudinal range. This region has been selected to be close to the GS and, at the same time, to avoid relatively high latitudes. Indeed, the Rossby wave detection is particularly challenging at those latitudes, as shown by the small number of studies on Rossby waves at latitudes higher than 39°N (e.g., Osychny and Cornillon 2004; Sasaki and Schneider 2011; Watelet et al. 2020). However, the general features of Rossby wave propagation discussed in later sections are rather insensitive to data averaged in latitudinal ranges between 32° and 38°N or in latitudinal ranges with an extension of 1°–3°.

The forcing of Rossby waves by the NAO has been assessed through the Hovmöller diagram of the bandpass-filtered wind stress curl anomalies averaged in the 35°–37°N latitudinal range. This latitudinal range is smaller than the one used for SST and SSH anomalies to avoid artefacts in the wind stress curl pattern induced by the presence of Azores Islands at 25°W (not shown).

Last, the NAO influence on the GSF latitudinal position through buoyancy forcing in the Labrador Sea has been assessed by analyzing the zonal oceanic transport along the Slope Sea. First, the zonal oceanic transport has been averaged along the 50°–68°W longitudinal range, where the GSF index has been defined. Then, the zonal transport has been integrated in the 43.5°–45°N latitudinal range and over the depth interval from 1000 to 3000 m (refer to the black box in Fig. S2 in the online supplemental material). The sign of the integrated transport has been inverted in order to have positive values for westward transport. The latitude–depth box has been selected to include the core of the subsurface oceanic transport along the Slope Sea during the winter season. This box coincides with the core of the DWBC transport. This is shown by the location of the potential vorticity minima generally used as a tracer to identify the signature of the DWBC (Fig. S2; Talley and McCartney 1982). For this reason, the index has been referred to as the DWBC index. It is specified that the meridional component of the DWBC transport has not been taken into account because the oceanic currents along the continental shelf of North America north of the GSF (50°–68°W) are mainly zonally oriented (not shown).

4) LEAD–LAG RELATIONSHIP

The lead–lag relationships between the bandpass-filtered NAO, GSF, Ekman, and DWBC indices have been assessed performing the lead–lag cross-correlation analysis. The statistical significance of the lead–lag cross correlations has been assessed through bootstrap test (Ebisuzaki 1997) against the null hypothesis of no correlation at the 95% confidence level. The bootstrap test has been performed by randomly resampling one of the two time series 1000 times.

Last, a lead–lag linear regression analysis based on the bandpass-filtered NAO index has been applied to bandpass-filtered Ekman transport in the North Atlantic and westward transport data along the Slope Sea to extract the respective response to the NAO forcing. The statistical significance of lead–lag linear regression coefficients has been assessed through a two-tailed Student's t test against the null hypothesis of coefficients equal to zero at the 90% confidence level.

3. Results

Both the NAO–GSF cross-wavelet power spectrum and the squared wavelet coherence show statistically significant values in the period range of 6–11 years and during 1972–2018 (Fig. 1). The peak at the decadal time scale is also present both in the single NAO and GSF wavelet and global wavelet power spectra (Figs. 2 and 3), providing further evidence of the NAO–GSF interaction. However, the peak in the GSF wavelet power spectrum is statistically significant only from 1985 onward.

In the context of the decadal NAO–GSF interaction during 1972–2018, the spectral features of the cross-wavelet power spectrum are homogeneous in time, whereas those of the squared wavelet coherence change around 1990. Indeed, before 1990 the squared wavelet coherence is statistically significant only for periods close to 11 years, with a phase relationship between the NAO and GSF time series of about 80° on average. In contrast, after 1990 the squared wavelet coherence is statistically significant in the decadal range (period range of 6–11 years), with a phase relationship between the two time series of about 120° on average. These results indicate that the lead–lag relationship between the NAO and the GSF at the decadal time scale changes in time. Specifically, the NAO leads the GSF shifts by about 3 years during 1972–90 and by 2 years during 1990–2018. Consistently, the lead–lag cross correlation between the bandpass-filtered NAO and GSF indices shows a peak when the former leads the latter by about 3 years during 1972–90 and by about 2 years during 1990–2018 (Fig. 4).

In the last part of the analyzed record (2005–15), both the NAO–GSF cross-wavelet power spectrum and the squared wavelet coherence show statistically significant values at periods shorter than 6 years, with the two time series closely in antiphase (Fig. 1). This covariability peak is associated with statistically significant values also in the individual wavelet power spectra for the NAO and GSF (Figs. 2 and 3). These results show that the NAO and the GSF covary at frequencies higher than the decadal one but only for a limited period of time. Consistently, the covariability peak at high frequencies during 2005–15 is associated with low power in both the NAO and GSF global wavelet power spectra (Figs. 2c and 3c).

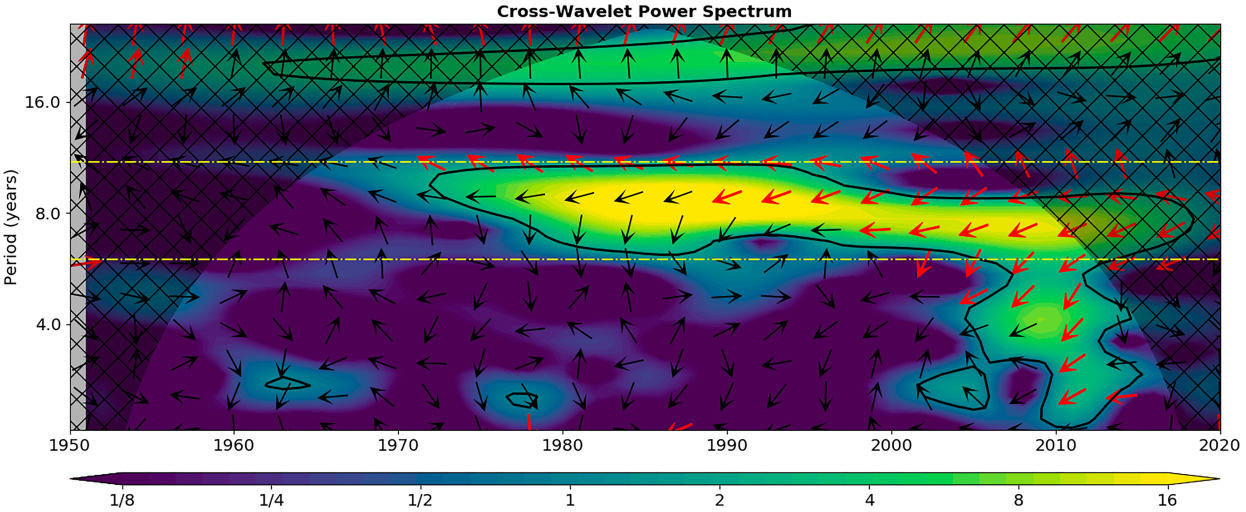

FIG. 1. Cross-wavelet transform of the detrended and standardized winter GSF and NAO time series. Thick black contours enclose the cross-wavelet power spectrum values that are statistically significant at the 90% confidence level. The phase relationship between the winter GSF and NAO time series is indicated by the vectors, following the convention in Torrence and Webster (1999). In the case of in-phase signals, vectors point upward; in the case of antiphase signals, vectors point downward. If the GSF leads the NAO, vectors point to the right; if the NAO leads the GSF, vectors point to the left. Thick red vectors indicate phase relationship in which squared wavelet coherence is statistically significant at the 90% confidence level (Kohyama et al. 2021). The lower and upper dot–dashed yellow lines represent the 6- and 11-year periods, respectively. Cross-hatched light shades indicate the cone of influence where edge effects may alter the power spectrum.

Last, another peak of covariability emerges at periods longer than 16 years (Fig. 1). However, the portion of the time–frequency phase space for periods longer than 16 years is largely affected by edge effects of the cross-wavelet analysis, so results in this time–frequency region should be considered with caution. Furthermore, this peak in the cross-wavelet power spectrum is associated with a peak in the wavelet power spectrum of the GSF time series, but not for the NAO (Figs. 2 and 3). This suggests that the NAO–GSF covariability at periods longer than 16 years could be an artifact of the strong variability of the GSF alone at these time scales (Maraun and Kurths 2004).

The cross-wavelet analysis has been repeated using ORAS5 (1958–2018; Zuo et al. 2019) and version 3.4.2 of the Simple

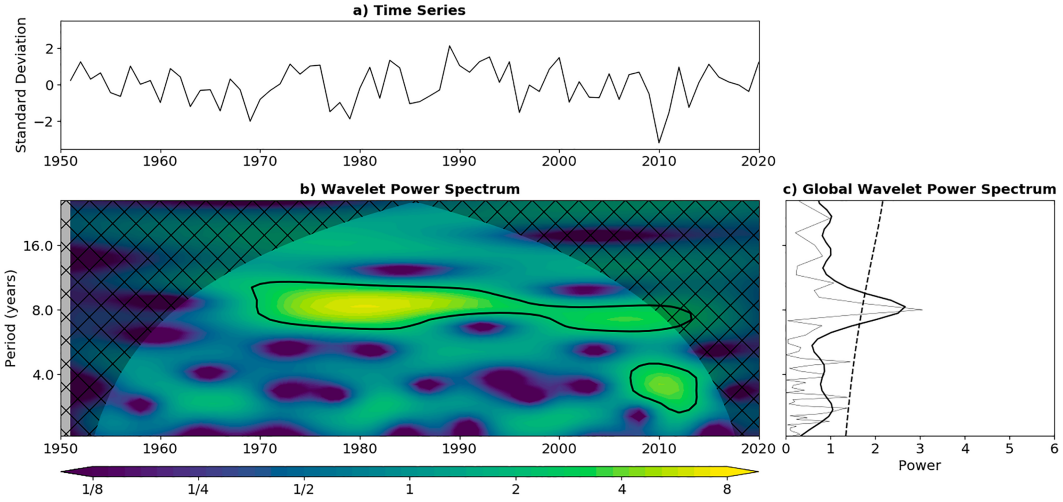

FIG. 2. (a) Detrended and standardized winter NAO time series in the ERA5 dataset (1950–2020). (b) Wavelet transform of the winter NAO time series. Thick black contours enclose the wavelet power spectrum values that are statistically significant at the 90% confidence level. Cross-hatched light shades indicate the cone of influence where edge effects may alter the power spectrum. (c) Global wavelet (thick line) and Fourier (thin line) power spectrum of detrended and standardized winter NAO time series. The thick dashed line represents the 90% confidence level of the time-averaged white-noise spectrum.

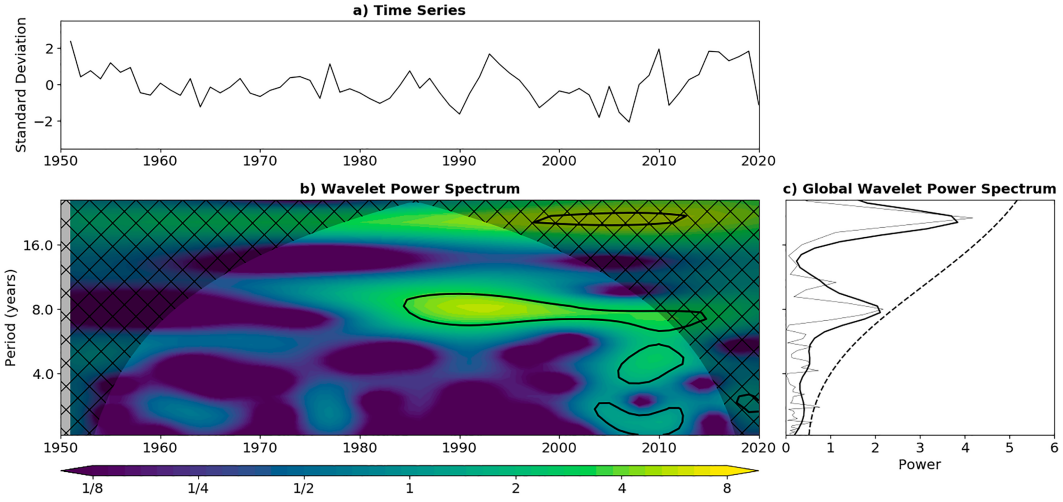

FIG. 3. As in Fig. 2, but for the winter GSF time series. In this case, the thick dashed line in (c) represents the 90% confidence level of the time-averaged red-noise spectrum.

Ocean Data Assimilation (SODA3.4.2; 1980–2020; Carton et al. 2018) as alternative ocean reanalyses. The general features of the NAO–GSF covariability described above are captured by both datasets (Figs. S3 and S4 in the online supplemental material), despite the SST biases over the GS region in the ORAS5 reanalysis and the limited time period covered by the SODA3.4.2 reanalysis. Indeed, both reanalyses show a statistically significant peak in the NAO–GSF cross-wavelet power spectrum at the decadal time scale. SODA3.4.2 also shows a statistically significant peak in the NAO–GSF squared wavelet coherence at the same time scale, with the NAO leading the GSF by about 2 years. In the ORAS5 reanalysis, the NAO–GSF covariability is confined during 1965–2012, in agreement with the results from ERA5 reanalysis. Furthermore, both reanalyses show a peak in the NAO–GSF covariability for periods shorter than 6 years after 2000 (Figs. S3 and S4). In the SODA3.4.2 reanalysis, the peak in the NAO–GSF cross-wavelet power spectrum for periods longer than 16 years is also present. Thus, the cross-wavelet analysis applied to ORAS5 and SODA3.4.2 reanalysis datasets provide further evidence of the decadal NAO–GSF covariability.

In order to assess the ocean–atmosphere interaction at the decadal time scale, the data and the selected indices have been bandpass filtered over the period range of 6–11 years. Note that we have only used the time period where the decadal peak is present in the ERA5 dataset (1972–2018) in the analyses described below. As mentioned in section 1, the NAO can force changes in the GSF latitudinal position through the anomalous basin-scale wind forcing and the buoyancy forcing over the

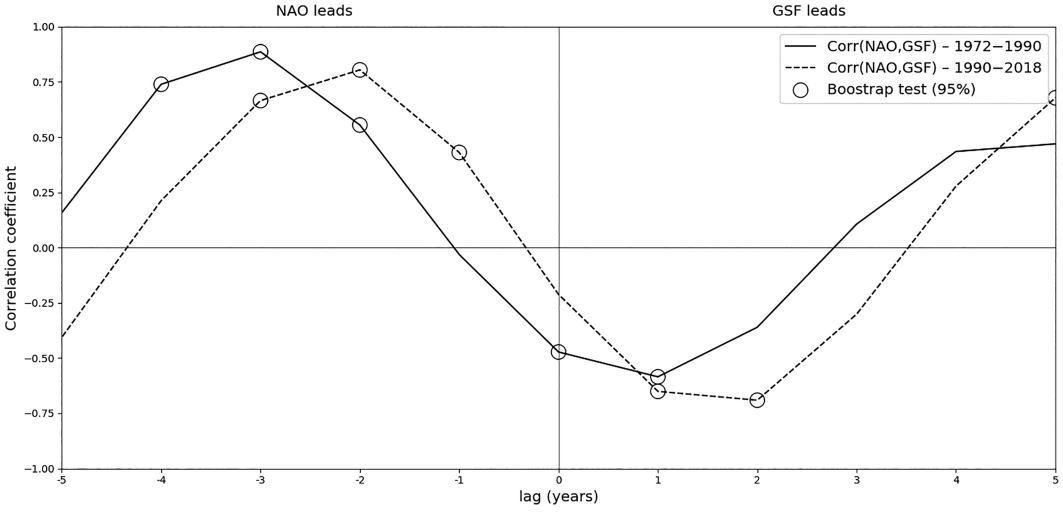

FIG. 4. Lead–lag cross correlation between the bandpass-filtered NAO and GSF indices during 1972–90 (solid) and 1990–2018 (dashed). The circles highlight the lead–lag cross correlations that are statistically significant against the null hypothesis of no correlation at the 95% confidence level.

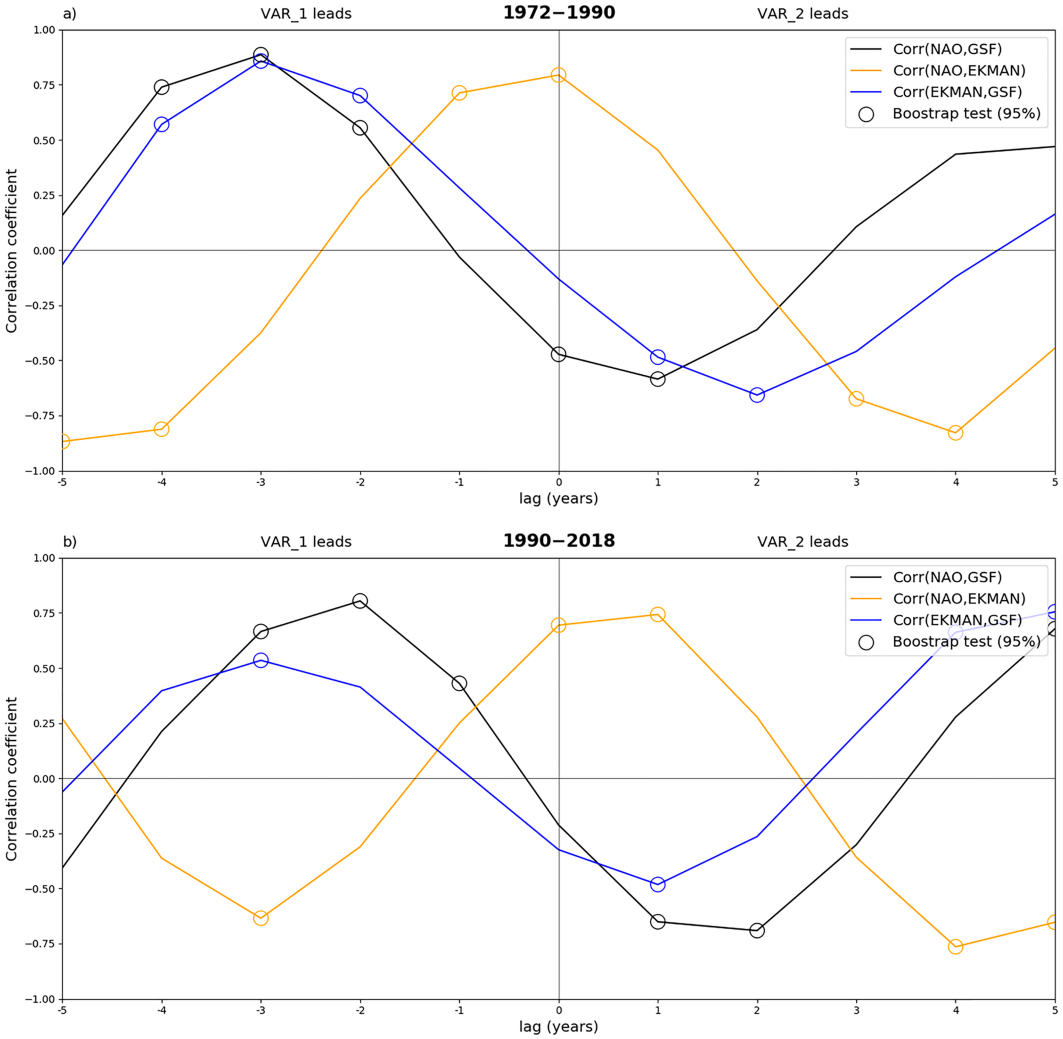

FIG. 5. Lead–lag cross correlation between the bandpass-filtered NAO, GSF and Ekman indices during (a) 1972–90 and (b) 1990–2018: NAO–GSF (black), NAO–Ekman (yellow), and Ekman–GSF (blue). The first variable leads in the left portion of the plot, and the second variable leads in the right portion of the plot. The Ekman index has been defined as the meridional Ekman transport averaged over the GSF area (50°–68°W, 35°–40°N). The circles highlight the lead–lag cross correlations that are statistically significant against the null hypothesis of no correlation at the 95% confidence level.

Labrador Sea (Taylor and Stephens 1998; Joyce et al. 2000; Rossby and Benway 2000; Hameed and Piontkovski 2004; Zhang and Vallis 2006; Joyce et al. 2019; Watelet et al. 2020). Here, we assess the response of the wind-driven oceanic circulation to the anomalous NAO wind stress, the excitation of Rossby waves, and the response of the westward flow along the Slope Sea to the NAO-related buoyancy forcing over the Labrador Sea. The assessment is performed over the individual time intervals of 1972–90 and 1990–2018, separately. The objective is to verify which mechanism can explain the observed lags between the GSF shifts and the NAO forcing on the decadal time scale and whether any of these mechanisms can account for the changes in the lead–lag NAO–GSF relationship between the two periods of time.

The lead–lag cross correlations between the bandpass-filtered NAO and Ekman indices show maximum values around lag 0 in both time periods (Fig. 5). Specifically, a positive or negative NAO phase is respectively associated with northward or southward Ekman transport anomalies over the GS area. The effect of the NAO forcing on the Ekman transport extends over the whole North Atlantic basin, with particularly intense anomalies in the subpolar gyre and the subtropical North Atlantic (Figs. 6 and 7). This is consistent with previous studies showing the instantaneous impact of the NAO-related wind stress on the wind-driven circulation in the North Atlantic (Visbeck et al. 2003; Deser et al. 2010). Since the wind-driven oceanic circulation adjusts quickly to the wind forcing, the negative peak in the NAO–Ekman transport cross correlation when the

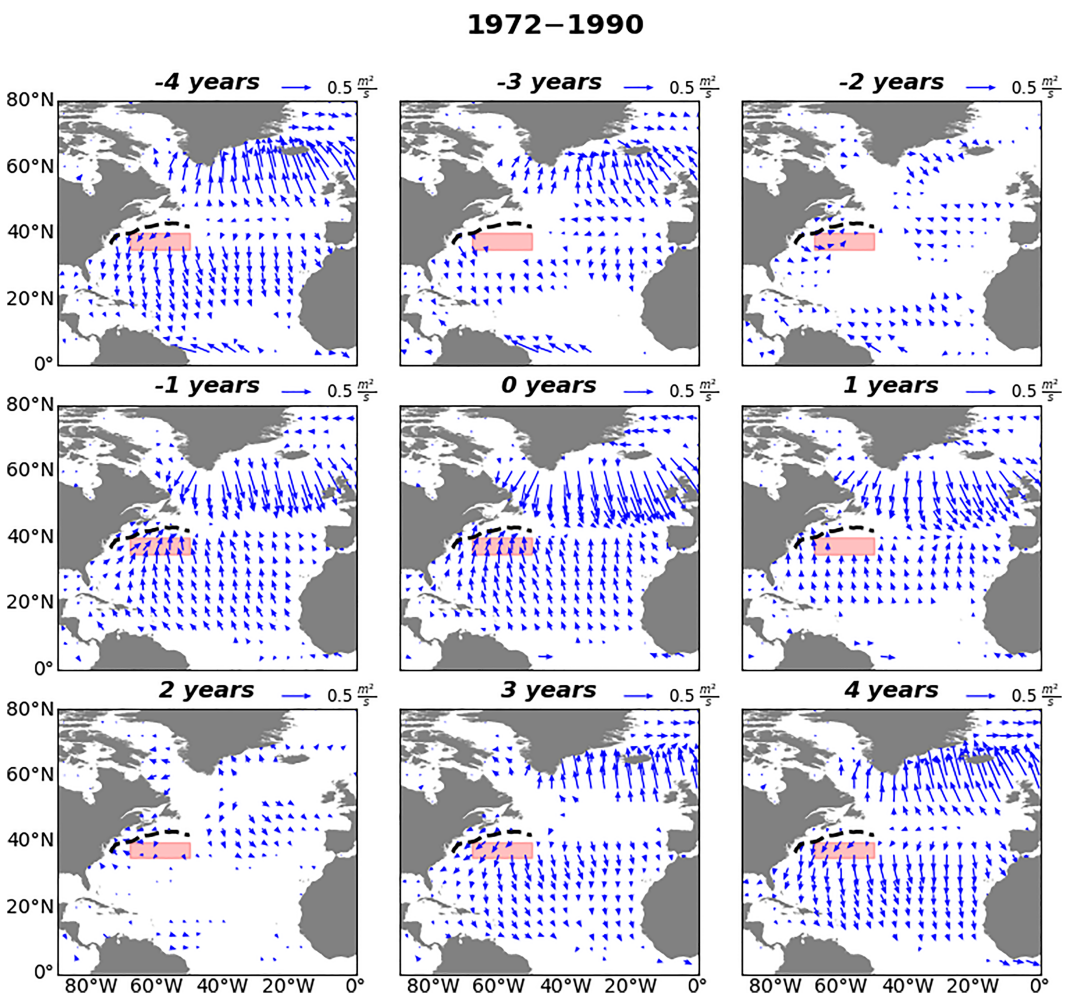

FIG. 6. Lead–lag linear regression coefficients for bandpass-filtered Ekman transport anomalies ($m^2\ s^{-1}$; arrows) on the bandpass-filtered NAO index in the winter season during 1972–90. Only regression coefficients for bandpass-filtered Ekman transport anomalies that are statistically significant against the null hypothesis of coefficients equal to zero at the 90% confidence level are shown. The NAO leads at negative lags and lags at positive lags, as in Fig. 5 (orange line). The winter climatological position of the GSF is indicated by the black dashed line. The red box represents the area where the meridional Ekman transport has been averaged to define the Ekman index (50°–68°W, 35°–40°N).

NAO leads the Ekman transport can be understood as the effect of the periodicity in the time series due to the bandpass filtering.

The fast response of the wind-driven oceanic circulation to the NAO forcing also determines that the Ekman transport leads the GSF shifts by the same number of years as the NAO. This is true for the 1972–90 interval, during which the Ekman transport–GSF and NAO–GSF cross correlations reveal the same lead–lag covariability pattern (Fig. 5a). It is not completely so during 1990–2018, when the anomalous Ekman transport seems to anticipate the NAO forcing by 1 year (Fig. 5b). This aspect shows that the variability of Ekman transport over the GS area may be also influenced by other factors besides the NAO. Furthermore, it implies an oceanic forcing of the NAO. Apart from that, the Ekman transport covaries with the NAO and thus, as expected, cannot account for the [2–3]-year time lag in the cross correlation between the GSF and NAO indices. Furthermore, results show that the Ekman mechanism cannot account for the changes in the lead–lag NAO–GSF relationship before and after 1990, this mechanism being active both during 1972–90 and 1990–2018.

The Hovmöller diagram (Hovmöller 1949) of the bandpass-filtered SST and SSH anomalies averaged in the 35°–38°N latitudinal range shows Rossby wave–like structures propagating from the eastern to western North Atlantic before 1990 (Fig. 8). The signal is particularly clear in the SST anomalies, whereas it appears noisier in the SSH anomalies. Positive or negative SST and SSH anomalies in eastern North Atlantic are respectively associated with negative or positive wind stress curl anomalies in the same Atlantic region (20°–35°W; Figs. S5 and S6 in the online supplemental material). Furthermore, negative or positive wind stress curl anomalies in the eastern North Atlantic are respectively associated with the positive or negative NAO

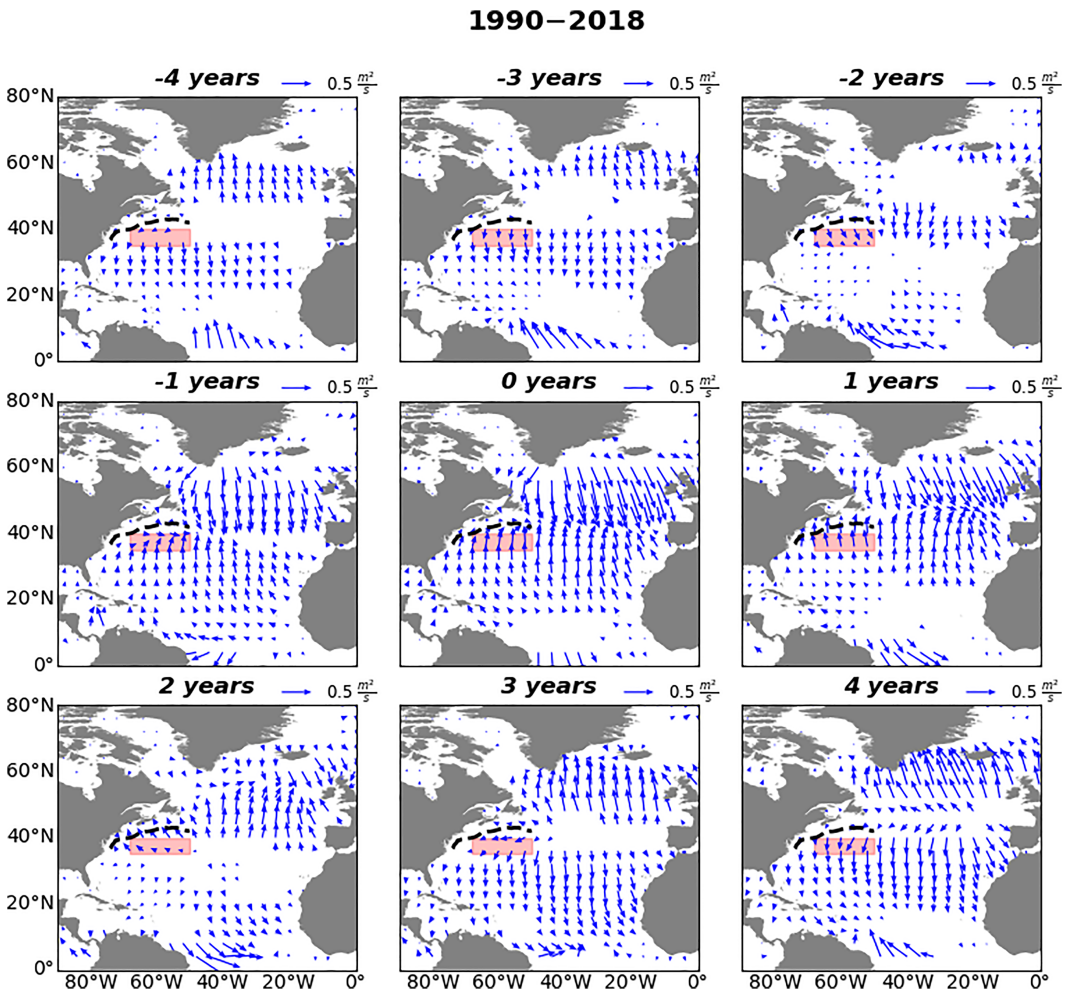

FIG. 7. As in Fig. 6, but during 1990–2018.

phase. This is consistent with previous studies showing that baroclinic Rossby waves can be excited by the anomalous Ekman convergence/divergence due to large-scale atmospheric circulation anomalies, such as those associated with the NAO (Anderson and Gill 1975; Sturges and Hong 1995; Sturges et al. 1998; Fu and Qiu 2002; Zhang et al. 2016; Årthun et al. 2021; Kowalski 2022). In this context, it has been shown that the momentum transfer between the atmosphere and the ocean is particularly intense around 30°W (Visbeck et al. 1998; Esselborn and Eden 2001). Consistently, the SST and SSH anomalies show maximum values between 25° and 35°W in the period where there is evidence of Rossby wave propagation (Fig. 8).

Once excited in the eastern North Atlantic, the positive or negative SST and SSH anomalies reach the western North Atlantic about 2–3 years later, respectively coinciding with a northward or southward shift of the GSF. Taking into account the distance between 30°W (as reference for the NAO-related perturbation initiating the Rossby waves) and 59°W (the center of the longitudinal range used to define the GSF latitudinal position), the time lag of 2–3 years corresponds to a phase speed of about 2.6–4 cm s^{-1}. These values are consistent with the phase speeds of baroclinic Rossby waves in extratropical North Atlantic proposed by previous studies (Cipollini et al. 1997, 2001; Osychny and Cornillon 2004; de Coëtlogon et al. 2006; Watelet et al. 2020). It is specified here that the general characteristics of the Rossby waves described above do not change applying a Lanczos 6-year low-pass filter (not shown), showing that the presence or absence of Rossby waves propagation is not significantly affected by the length of time filtering.

The results above support the idea of the NAO affecting the GSF latitudinal position through Rossby wave excitation, but only before 1990. As specified before, the spectral features of the decadal NAO–GSF covariability in this period are different than those from 1990 onward (Fig. 1). Thus, the differences in the spectral features of the decadal NAO–GSF interaction before and after 1990 may be induced by the nonstationarity of the Rossby wave propagation. The evidence of Rossby wave propagation for a limited period of time is consistent with results by Sasaki and Schneider (2011), showing westward wave propagation only during 1965–85. After 1990, the SST anomalies

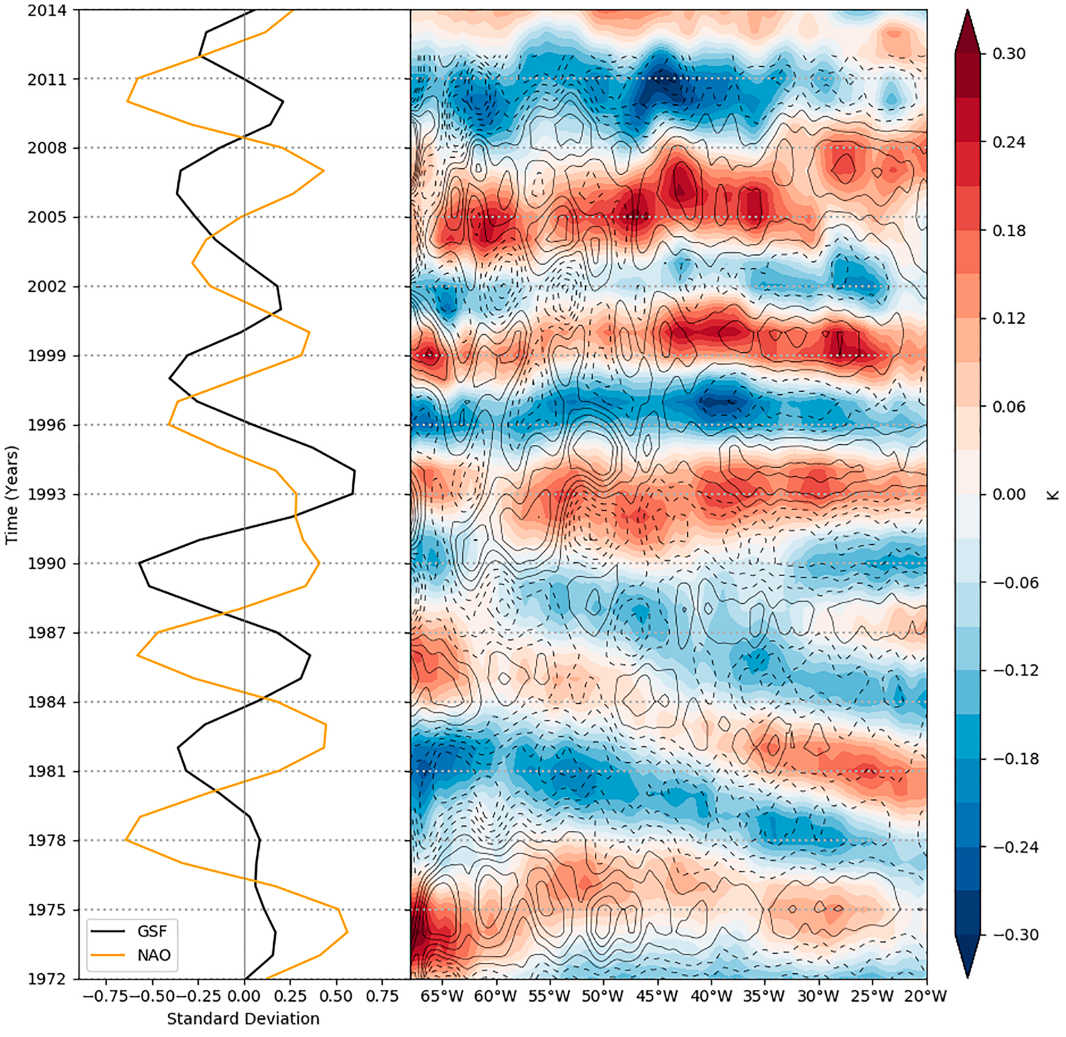

FIG. 8. (left) Bandpass-filtered winter GSF (black) and NAO (orange) time series between 1972 and 2014. (right) Hovmöller diagram of the bandpass-filtered SST (K; color shading) and SSH anomalies (cm; black contours, with contours every 0.5 cm from −1.75 cm) averaged in the 35°–38°N latitudinal range during 1972–2014. It is specified that 6 years are lost at each border of the time series because of the application of the Lanczos filter (see detail in section 2). For this reason, the *y* axis of the plot ranges from 1972 up to 2014 and not from 1972 up to 2018, that is, when the GSF and NAO covary at the decadal time scale (Fig. 1). The SSH time series are even shorter because the original SSH data are provided until 2018.

show no propagation, with anomalies changing their sign in agreement with the NAO forcing. The reasons behind the absence of Rossby wave propagation after 1990 are unclear. However, refer to section 4 for a brief discussion about possible explanations of nonstationarity in this mechanism.

The results above also show that, unlike the Ekman transport, the Rossby wave propagation mechanism may be important in setting the time lag between the NAO and the GSF position changes, particularly before 1990. This is thought to be the case because the 3-year time lag between the NAO and the GSF shifts is about the same as the time required for SST and SSH anomalies generated in the central and eastern North Atlantic to propagate westward across the basin (Fig. 8).

Last, the NAO can influence the GSF latitudinal position through buoyancy forcing over the Labrador Sea, affecting the export of Labrador Sea Water and thus the southwestward flow along the Slope Sea (Joyce et al. 2000; Rossby and Benway 2000; Hameed and Piontkovski 2004; Zhang and Vallis 2007).

Figure 9 shows that maximum positive correlation between the bandpass-filtered NAO and DWBC indices is found when the former leads the latter by 4 years. This is true during both 1972–90 and 1990–2018. Specifically, the positive or negative NAO respectively enhances or reduces the westward volume transport along the Slope Sea after 4 years, with anomalies extending to a depth of 3000 m and reaching the greatest amplitude at the depth of the DWBC core (depth of 1000–3000 m; Figs. 10 and 11). These deep-water transport anomalies can

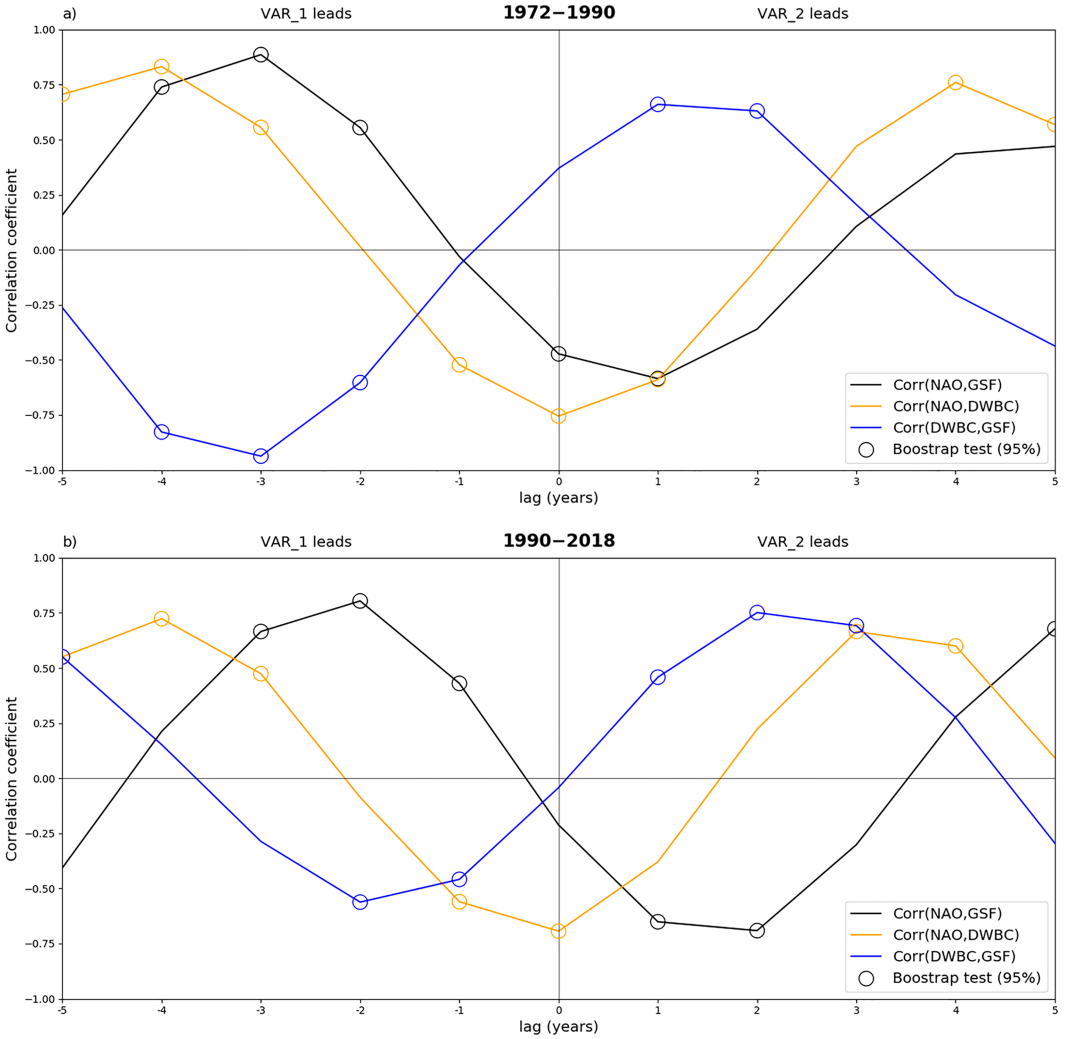

FIG. 9. Lead–lag cross correlation between the bandpass-filtered NAO, GSF, and DWBC indices during (a) 1972–90 and (b) 1990–2018: NAO–GSF (black), NAO–DWBC (yellow), and DWBC–GSF (blue). The first variable leads in the left portion of the plot, and the second variable leads in the right portion of the plot. The DWBC index has been defined as the total oceanic westward transport in the 43.5°–45°N latitudinal range and 1000–3000 m depth (the black dash-outlined box in Fig. S2 in the online supplemental material). The circles highlight the lead–lag cross correlations that are statistically significant against the null hypothesis of no correlation at the 95% confidence level.

be associated with the heat loss or heat gain over the Labrador Sea during a positive or negative NAO phase, respectively (not shown), which is expected to affect the formation (through deep convection) and, ultimately, the export of Labrador Sea Water via the DWBC. In this context, it is specified that the anomalies in the zonal flow along the Slope Sea are more intense during 1990–2018 (Fig. 11). Furthermore, statistically significant anomalies appear at depths greater than 3000 m during 1972–90 (Fig. 10). These water masses are generally referred to as Overflow Water (i.e., the densest branch of the DWBC) and previous studies have shown that they are formed in the Greenland and Norwegian Seas (Worthington 1976; Pickart 1992). Therefore, the NAO-related buoyancy forcing over the Labrador Sea is expected to play no role for the transport anomalies deeper than 3000 m.

The 4-year time lag between the response of the DWBC and the NAO forcing is consistent with the range of values shown in previous observational and modeling studies. Zhang and Vallis (2006) have shown that changes in the deep convection in the Labrador Sea lead anomalies in the NRG intensity by 4 years, which is the time for the DWBC variations to propagate from the Labrador Sea to the Grand Banks with the advection speed. In agreement with this, Peña-Molino et al. (2011) have shown that anomalies in the uppermost layer of the DWBC (500–1000 m depth approximately) take about 4–7 years to reach the GS area. Georgiou et al. (2020) have shown that most of the dense water formed by deep convection in the Labrador Sea exits the subpolar basin through indirect routes that involve exchanges between the boundary currents and the ocean interior. Such

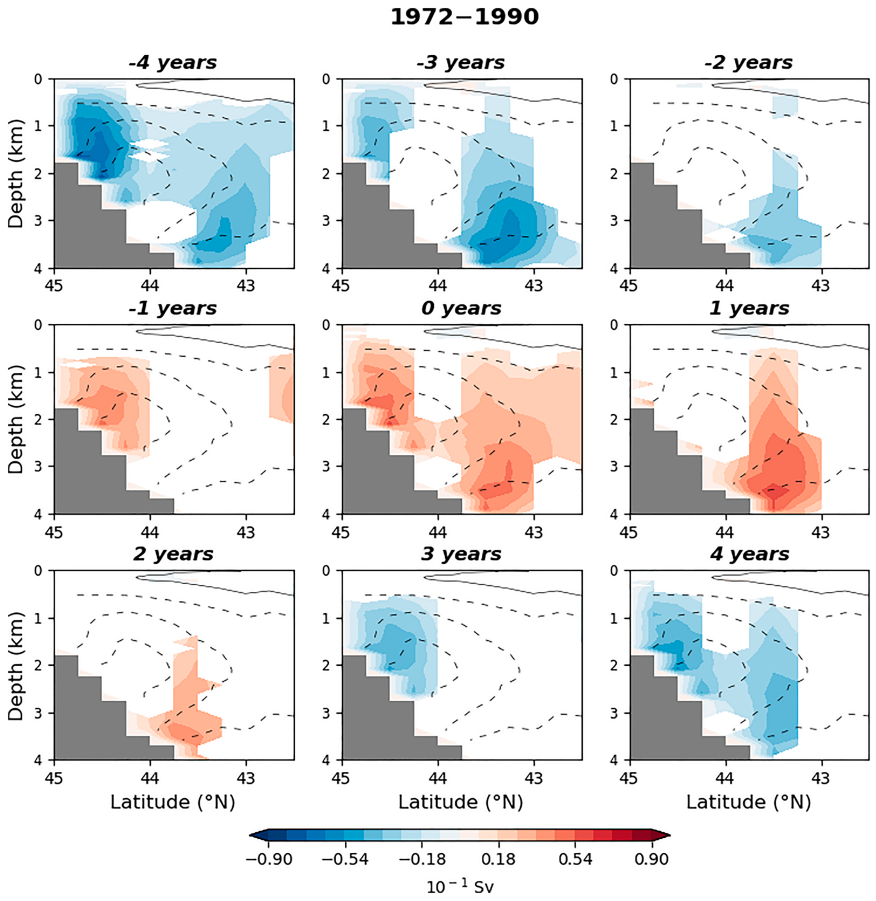

FIG. 10. Lead–lag linear regression coefficients for bandpass-filtered zonal transport anomalies [10^{-1} Sv (1 Sv $\equiv 10^6$ m^3 s^{-1}); color shading] on the bandpass-filtered NAO index in the winter season during 1972–90. The zonal transport anomalies have been averaged in the 50°–68°W longitudinal range before performing the linear regression. Only regression coefficients that are statistically significant against the null hypothesis of coefficients equal to zero at the 90% confidence level are shown. Gray contours indicate the winter climatology of the zonal oceanic transport every 10^{-1} Sv from -3×10^{-1} Sv. The NAO leads at negative lags and lags at positive lags, as in Fig. 9 (orange line).

routes are associated with export time scales that are usually between 1 and 6 years.

Furthermore, Fig. 9 shows intense negative correlation between the bandpass-filtered NAO and DWBC indices at lag 0 during both 1972–90 and 1990–2018. Specifically, the positive (negative) NAO is associated with the concomitant reduction (enhancement) of the westward volume transport along the Slope Sea. The fast DWBC response to the atmospheric forcing is consistent with previous modeling studies showing that AMOC variations induced by buoyancy forcing over the Labrador Sea can propagate southward through rapid coastal Kelvin wave, reaching the equator in less than 1 year (Johnson and Marshall 2002; Getzlaff et al. 2005; Zhang 2010). In this context, Zhang (2010) has shown that strong positive salinity anomalies in the Labrador Sea are associated with the reduction of DWBC transport along the eastern continental shelf of North America (refer to their Fig. 4), similar to what is shown in Figs. 10 and 11.

Thus, Fig. 9 suggests that the southwestward flow anomalies along the Slope Sea may be interpreted both as variations in the deep oceanic circulation that quickly travel southward through fast coastal Kelvin waves and as a delayed oceanic response with deep oceanic circulation anomalies traveling southward with the advection speed. This is consistent with the study by Zhang (2010), which has proposed that the southward propagation of AMOC anomalies induced by buoyancy forcing over the Labrador Sea is in two stages: a first stage characterized by a fast Kelvin wave response and a second stage characterized by a slow response in which the anomalies are advected southward by the mean flow.

To better understand the southward propagation of NAO-induced AMOC anomalies, we have performed a lead–lag linear regression analysis of the bandpass-filtered AMOC anomalies onto the bandpass-filtered NAO index. Similar to Zhang (2010), the AMOC at each latitude has been defined as the maximum of the meridional overturning streamfunction in the density

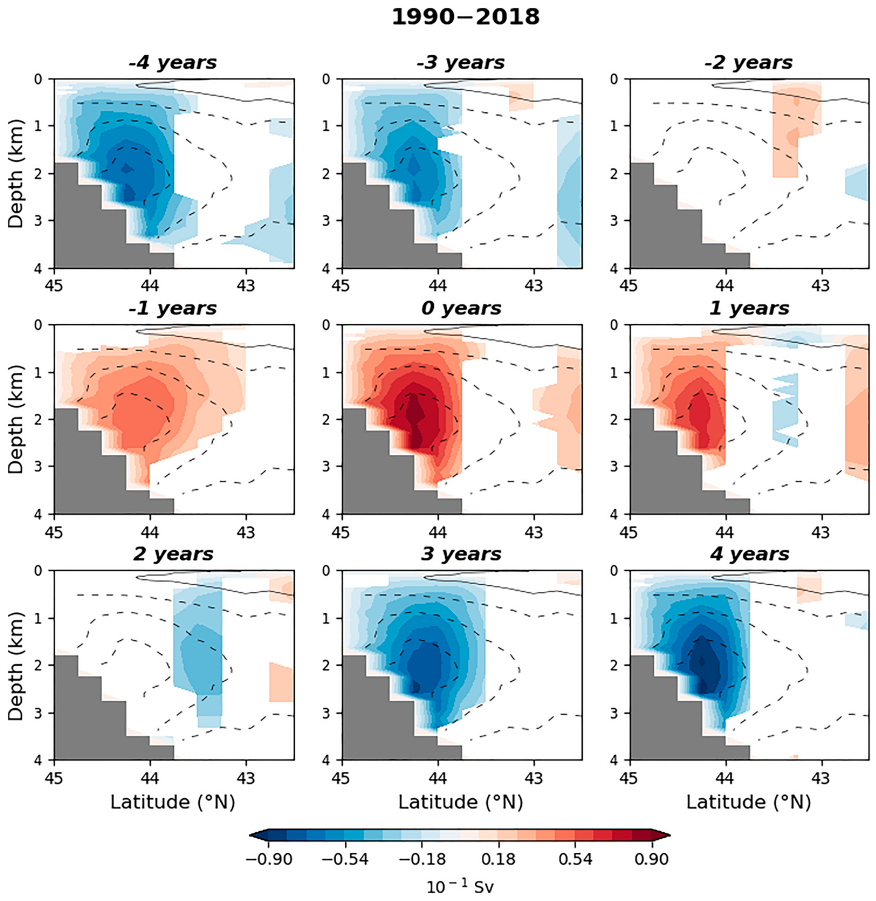

FIG. 11. As in Fig. 10, but during 1990–2018.

space during the winter season. The linear regression has been performed over the entire time period 1972–2018, as the NAO–DWBC interaction is stationary over this period (Fig. 9; orange line). Figure 12 shows that the AMOC responds to the NAO forcing with a lag of about 3–4 years north of 40°–45°N, with coherent anomalies extending over a wide range of latitudes in the subpolar basin. Specifically, the most significant values are concentrated in the 50°–55°N latitudinal range, corresponding to the Labrador Sea region. Here, surface waters experience the strongest NAO-related surface atmospheric forcing, triggering deep convection. The delayed AMOC response to atmospheric forcing in the Labrador Sea is consistent with previous studies, linking this delay to the time it takes for deep water to adjust to wind forcing and exit the subpolar basin via slow indirect pathways (Eden and Greatbatch 2003; Getzlaff et al. 2005; Georgiou et al. 2020). After reaching 40°–45°N, the AMOC anomalies start to propagate southward, with a time scale consistent with the mean flow advection. In particular, the AMOC anomalies reach the subtropical North Atlantic at 30°N after 2–3 years, lagging the NAO forcing by about 6–7 years. In this context, it is specified that the linear regression coefficients are statistically significant (at the 90% confidence level) only up to about 37°N. Nonetheless, a slow propagation of the AMOC anomalies toward the equator is still detectable, with a time scale in line with Zhang (2010). South of 30°N, the weak coefficients suggest a much faster propagation, reaching 20°N in less than 1 year. This is consistent with AMOC anomalies traveling along the eastern North America seaboard through coastally trapped Kelvin waves, in agreement with Zhang (2010) and Johnson and Marshall (2002). Apart from this delayed response, Fig. 12 also shows significant regression values south of 35° in the lag interval of 0–2 years. These anomalies cannot be interpreted as the signature of fast-propagating Kelvin waves, because they lead the positive NAO-forced AMOC anomalies in the Labrador Sea region by 2–3 years. Moreover, they are associated with concurrent opposite AMOC anomalies at higher latitudes. Instead, these anomalies may capture the local/quasi-instantaneous adjustment of subtropical North Atlantic basin to the NAO forcing, as suggested by previous studies (e.g., Joyce et al. 2000). Further in-depth analyses are required to provide a comprehensive explanation of the subtropical deep oceanic response to NAO forcing. Nevertheless, overall Fig. 12 confirms that the NAO-induced AMOC anomalies travel southward on a time scale consistent with the mean flow, whereas it does not show clear evidence for the role played by Kelvin waves.

Figure 9 shows a negative peak in the cross correlation between the DWBC and GSF indices when the former leads the

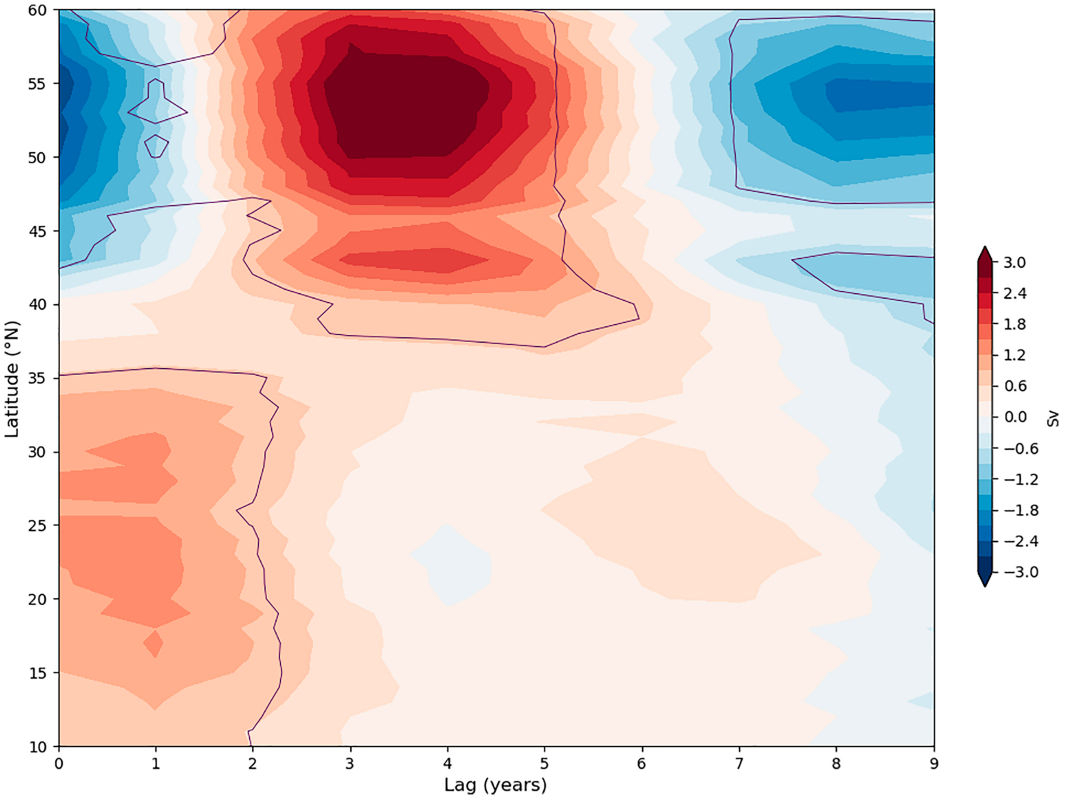

FIG. 12. Linear regression coefficients for bandpass-filtered AMOC anomalies (Sv; color shadings) on the bandpass-filtered NAO index in the winter season during 1972–2018. The AMOC at each latitude has been defined as the maximum of the meridional overturning streamfunction in the density space during the winter season. The lags on the *x* axis indicate the number of years by which the winter NAO leads the AMOC anomalies. Black contours enclose the coefficients that are statistically significant against the null hypothesis of coefficients equal to zero at the 90% confidence level.

latter by 3 years during 1972–90 and by 2 years during 1990–2018. This means that the GSF shifts northward (southward) after the westward DWBC transport is reduced (intensified). This is consistent with the fact that the stronger (weaker) DWBC transport is expected to be associated with stronger (weaker) bottom vortex stretching along the Slope Sea and thus with a more (less) intense NRG (Zhang and Vallis 2006, 2007). The equivalent barotropic nature of the anomalous westward flow along the Slope Sea (Figs. 10 and 11) is the signature of the changes in the NRG. In this context, the anticyclonic (cyclonic) barotropic streamfunction anomalies over the GS region have been shown to peak about 2 years after the intensification (reduction) of the DWBC transport along the Slope Sea (Zhang 2010). This 2-year time lag is consistent with the one between the DWBC and GSF indices during 1990–2018 in Fig. 9b. Thus, results suggest that the DWBC mechanism can directly account for the time lag between the GSF and NAO indices after 1990. Differently, the time lag between the DWBC and GSF indices during 1972–90 is 1 year longer than what expected from this mechanism. However, the lead–lag relationship between the NAO and DWBC indices is stationary over the entire time period 1972–2018 (Fig. 9; orange line). This means that the NAO forces DWBC anomalies both during 1972–90 and 1990–2018 and that the DWBC mechanism is always active. Thus, the differences in the time lag between the DWBC and GSF indices before and after 1990 cannot be explained as an effect of the temporal modulations of the DWBC mechanism by itself. Differently, results suggest that the effect of the DWBC transport on the GSF latitudinal position could be modulated by other factors before 1990, with consequent effect on the lead–lag NAO–GSF relationship.

Despite these pieces of evidence, the role played by the anomalous DWBC transport of the GSF latitudinal position should be interpreted with caution. Indeed, there are still some concerns in literature about the effective role that coastal Kelvin waves have on the southward propagation of AMOC variations. Furthermore, the filtering of data applied here make difficult the interpretation of the causal link between the NAO forcing, the DWBC response, and the GSF shifts. Refer to section 4 for more discussion about these aspects.

4. Discussion

Results described in the previous section show that, in the ERA5 dataset, the NAO and GSF indices covary at the decadal time scale during 1972–2018 (Fig. 1). Over this time period, the year 1990 marks a discontinuity in the decadal

covariability of these two indices, with the NAO leading the GSF shifts by about 3 years during 1972–90 and by about 2 years during 1990–2018 (Fig. 4). It is here noted that other studies have also discussed a discontinuity in the air–sea interaction over North Atlantic occurring around 1990 (Andres et al. 2013; Kenigson et al. 2018; Diabaté et al. 2021). Specifically, the changes in the nature of NAO-related wind stress during the twentieth century have been suggested to cause a decadal shift of the relationship between the NAO and the interannual sea level variability along the eastern coast of North America. These results further support the existence of a discontinuity in the decadal air–sea interaction over the GS area during the 1990s.

Based on these pieces of evidence, we have assessed several mechanisms through which the NAO may be forcing the GSF latitudinal position on the decadal time scale. Specifically, we have inferred the responses of wind-driven Ekman and DWBC transport to the NAO forcing through lagged correlation analyses, and we have verified the presence of Rossby wave–like patterns excited by the NAO through the Hovmöller diagram of several bandpass-filtered atmospheric and oceanic variables in the extratropical North Atlantic. The final objective was to verify which mechanism can explain the time lags between the GSF shifts and the NAO forcing on the decadal time scale and whether any of these mechanisms can account for the changes in the lead–lag NAO–GSF relationship between the two periods of time mentioned above.

Results suggest that the response of Ekman transport to the NAO cannot directly account either for the lagged response of the GSF shift to the NAO or for the change in the NAO–GSF lead–lag relationship at the end of the 1990s (Fig. 5). However, this does not mean that this mechanism does not play any role in the evolution of the GSF shifts. Indeed, being active during the entire period 1972–2018, the anomalous Ekman transport in the GS region is thought to affect the tendency of the GSF latitudinal position together with the other mechanisms here analyzed. In contrast, the Rossby wave propagation mechanism appears to be consistent with the time lag between the NAO and the GSF response before 1990 (Fig. 8), while the response of the DWBC transport to the NAO forcing can account for the time lag between the NAO and the GSF response after 1990 (Fig. 9). However, the DWBC mechanism may also play a role in the evolution of the GSF latitudinal position before 1990, this mechanism being active during the entire period here analyzed.

In this context, the role played by the anomalous DWBC transport on the GSF latitudinal position requires further discussion. Results described in previous section show that the DWBC index lags the NAO index by about 4 years and that the anomalous DWBC transport along the Slope Sea induces the GSF shifts after about 2 years by affecting the NRG. If this is the case, we expect that the delayed DWBC/NRG response to a positive or negative NAO phase would tend to drive a southward or northward GSF shift, respectively, about 6 years after the NAO phase. Consistently, the correlation between the bandpass-filtered NAO and GSF indices shows significant negative values when the former leads the latter by 6 years during 1990–2018 (not shown). The 6-year time lag between changes in the deep oceanic circulation in the Labrador Sea and the GS meridional displacements has been also suggested by Zhang (2010). In the context of the present work, noting that there is a periodicity of about 8–9 years in the time series arising from the applied bandpass filter, we expect that the delayed DWBC response 4 years after a positive or negative NAO phase will start to affect the GSF latitudinal position during the following negative or positive NAO phase, respectively. This may explain why a positive peak in the correlation between the bandpass-filtered NAO and GSF indices emerges when the former leads the latter by 2 years during 1990–2018.

However, previous modeling studies have also suggested that AMOC variations associated with changes in deep oceanic circulation in the North Atlantic can propagate southward much faster, through rapid coastal Kelvin waves (Johnson and Marshall 2002; Getzlaff et al. 2005; Zhang 2010). If this is the case, taking into account the role played by the DWBC on the NRG, the concomitant DWBC response to the NAO forcing may directly explain the positive peak in the correlation between the bandpass-filtered NAO and GSF indices when the former leads the latter by 2 years. Although there is evidence from modeling studies that coastal Kelvin waves play a role in the southward propagation of AMOC variations, there are still some concerns about the effectiveness of this mechanism. This is because the simulated time for AMOC variations to propagate from high to low latitudes through coastal waves is much shorter than what observations suggest (less than 1 year vs more than 10 years; Smethie 1993; Molinari et al. 1998). This appears to be supported by Fig. 12, which shows that positive AMOC anomalies reach 30°N about 6–7 years after a positive NAO phase. Furthermore, the filtering of data applied here makes difficult the interpretation of the causal link between the NAO forcing and the DWBC response. In particular, the in-phase negative correlation between the NAO and DWBC indices (Fig. 9) could also be interpreted as the response of the DWBC transport along the Slope Sea 4 years after the previous (opposite) phase of the NAO. It is not possible to draw definitive conclusions in the context of the present paper. However, it may be that the DWBC response to the NAO forcing may be interpreted as variations in the deep oceanic circulation in the North Atlantic that quickly travel southward through fast coastal Kelvin waves (Johnson and Marshall 2002; Getzlaff et al. 2005; Zhang 2010) and/or as a delayed oceanic response with deep oceanic circulation anomalies traveling southward with the advection speed (Zhang and Vallis 2006; Peña-Molino et al. 2011).

Regardless of the mechanism by which anomalies in the deep oceanic circulation are forced by the NAO, the DWBC transport mechanism is active both during 1972–90 and 1990–2018 and hence it is suggested here that the differences in the lead–lag NAO–GSF relationship between the two time periods are induced by the nonstationarity of Rossby wave propagation. Indeed, the Rossby waves excited by a positive/negative NAO phase on the eastern North Atlantic require about 2–3 years to reach the GS area (Fig. 8). Thus, the Rossby wave propagation further extends the GSF shift induced by the anomalous DWBC transport alone. This increases the time lag between the NAO and the GSF response

respect the period 1990–2018, when the Rossby wave propagation is not active and the time lag is induced by the anomalous DWBC transport, and the associated anomalous NRG circulation, in response to the NAO forcing.

Before closing this section, the possible causes of the nonstationarity in the NAO–GSF relation and associated mechanisms will be discussed. First, it is important to consider that the quality of observational data has greatly improved during the last decades. In particular, the absence of the decadal NAO–GSF covariability before 1972 could be an artifact due to a lack of satellite observations during that time period rather than an effective independence between the two time series. The quality of data could also cause the discrepancies in the lead–lag NAO–GSF relationship before and after 1990. Satellite observations provide highly resolved SST data, which can capture GSF shifts of approximately 50–100 km. This was hardly possible with observational datasets before 1979. However, the limited length of satellite observations can put in question the spectral features of the NAO–GSF covariability, especially over decadal and multidecadal time scales.

Furthermore, it should be taken into account that the features of the decadal North Atlantic atmospheric variability can change in time. For example, it is here noted that the NAO index shows a peak of variability on the decadal time scale that is stronger during 1970–90 (Fig. 2). The changes in the character of the surface atmospheric forcing in time could affect the way the ocean responds to the forcing and thus the Rossby wave propagation. This idea is consistent with results by previous studies, showing that decadal changes in the NAO-related wind stress patterns occurring around 1990 could have affected the relationship between the NAO and the sea level variability along the coast of North America (Kenigson et al. 2018; Diabaté et al. 2021). In addition, it should be mentioned that the atmosphere undergoes decadal variability also projecting on other patterns largely orthogonal or/and independent to the NAO (Häkkinen et al. 2011; Årthun et al. 2021), which may also affect the oceanic circulation in the North Atlantic such as the Rossby wave propagation.

Last, it should be taken into account that the GS latitudinal position is potentially affected by a number of phenomena other than the NAO, such as the Atlantic meridional mode (Hameed et al. 2018; Wolfe et al. 2019), the Atlantic multidecadal oscillation (Nigam et al. 2018), the AMOC (de Coëtlogon et al. 2006; Joyce and Zhang 2010), and ENSO (Pérez-Hernández and Joyce 2014; Sanchez-Franks et al. 2016).

All of these aspects could be relevant to explain the dependency of the lead–lag NAO–GSF relationship over time as well as the lack of decadal NAO–GSF covariability before 1972. Further studies using longer time records of highly resolved SST data and high-resolution model experiments could be helpful to further assess the robustness of the nonstationarity in the NAO–GSF relation and deepen our understanding of its possible causes and the associated mechanisms.

5. Conclusions

The interaction between the NAO and the GSF latitudinal position has been the subject of extensive investigations. In this context, there are indications of nonstationarity in this interaction but the differences among methodologies used in prior studies make it difficult to draw consistent conclusions. Furthermore, there is a lack of consensus on the key mechanisms underlying the response of the GSF to the NAO. The goal of this study was to assess the possible nonstationarity in the NAO–GSF interaction and to help clarify the mechanisms underlying this interaction over the last few decades, using atmosphere and ocean reanalysis data.

Results show that the interaction between the NAO and the GSF latitudinal shifts during the winter season is nonstationary over the 1950–2020 time period. The NAO and GSF indices covary on the decadal time scale (period range of 6–11 years) but only during 1972–2018 (Fig. 1). A secondary peak in the NAO–GSF covariability emerges on multiannual time scales (periods shorter than 6 years) but only for a limited period of time (2005–15). The detection of these decadal and multiannual peaks in different reanalyses products provides robustness to this finding (Figs. S3 and S4 in the online supplemental material).

The nonstationarity in the decadal NAO–GSF covariability is also manifested through the dependency of their lead–lag relationship on the analyzed time period. Indeed, the NAO leads the GSF shifts by 3 years during 1972–90 and by 2 years during 1990–2018 (Fig. 4). Note that this may in part explain the discrepancies in the lead–lag relationships between the GSF and the NAO suggested in previous studies (Table 1). Depending on the analyzed time period, the lead–lag relationship between the GSF latitudinal position and its drivers may be different.

Overall, results show that the response of the GSF to the NAO on the decadal time scale can be interpreted as the joint effect of several different mechanisms, which are not all stationary across the 1972–2018 period. Before 1990, we interpret the response of the GSF to the NAO to reflect a combination of the quick Ekman transport response (Figs. 5a and 6), the DWBC transport response (Figs. 9a and 10), and the propagation of Rossby waves induced by the NAO forcing (Fig. 8), with the time lag between the NAO forcing and the GSF shifts being most consistent with the Rossby wave mechanism. After 1990, we find an absence of Rossby wave propagation and thus the overall response of the GSF to the NAO is influenced only by the responses of Ekman transport (Figs. 5b and 7) and DWBC transport (Figs. 9b and 11) to the NAO. In this case, the time lag between the GSF shifts and the NAO seems to be most consistent with the DWBC mechanism. Here it is suggested that the nonstationarity of the Rossby wave propagation causes the time lag between the NAO and the GSF latitudinal position on the decadal time scale to differ before and after 1990.

The nonstationarity in the NAO–GSF covariability has implications for predictability in the North Atlantic sector. Previous studies have proposed statistical models to predict the GS latitudinal position based on the atmospheric state some years in advance (e.g., Hameed and Piontkovski 2004; Sanchez-Franks et al. 2016). However, the relationship between the GS latitudinal position and the atmospheric indices has been generally considered stationary. Thus, results in the

present study indicate the potential inadequacy of statistical models that do not take into account the nonstationary character of the NAO–GSF interaction. Furthermore, considering the impact that the GSF shifts have on the North Atlantic atmospheric circulation (Joyce et al. 2019; Famooss Paolini et al. 2022), errors in predicting the GSF latitudinal position can reduce our skill in predicting the atmospheric variability through statistical and dynamical predictions (Athanasiadis et al. 2020).

Acknowledgments. Authors AB, PJA, and CRP received funding by from the Ministero dell'Università e Ricerca (MUR) (D.D. 1316; 8 June 2021) and the JPI Oceans and JPI Climate Joint Call 2019 "Next Generation Climate Science in Europe for Oceans" ROADMAP Project. Authors NEO and NK were supported through the Research Council of Norway (Grant 316618) that funded their contribution to ROADMAP.

Data availability statement. ERA5 reanalysis data are available on Copernicus Climate Data Store (CDS; https://cds.climate.copernicus.eu/#!/search?text=ERA5). ORAS5 reanalysis data are available from the Integrated Climate Data Center (Center for Earth System Research and Sustainability, University of Hamburg; https://www.cen.uni-hamburg.de/icdc). SODA reanalysis data are made available by the Department of Atmospheric and Oceanic Science at the University of Maryland (https://dsrs.atmos.umd.edu/DATA/soda3.4.2/REGRIDED/ocean/).

REFERENCES

Anderson, D. L. T., and A. E. Gill, 1975: Spin-up of a stratified ocean, with applications to upwelling. *Deep-Sea Res. Oceanogr. Abstr.*, **22**, 583–596, https://doi.org/10.1016/0011-7471(75)90046-7.

Andres, M., G. G. Gawarkiewicz, and J. M. Toole, 2013: Interannual sea level variability in the western North Atlantic: Regional forcing and remote response. *Geophys. Res. Lett.*, **40**, 5915–5919, https://doi.org/10.1002/2013GL058013.

Årthun, M., R. C. J. Wills, H. L. Johnson, L. Chafik, and H. R. Langehaug, 2021: Mechanisms of decadal North Atlantic climate variability and implications for the recent cold anomaly. *J. Climate*, **34**, 3421–3439, https://doi.org/10.1175/JCLI-D-20-0464.1.

Athanasiadis, P. J., S. Yeager, Y.-O. Kwon, A. Bellucci, D. W. Smith, and S. Tibaldi, 2020: Decadal predictability of North Atlantic blocking and the NAO. *npj Climate Atmos. Sci.*, **3**, 20, https://doi.org/10.1038/s41612-020-0120-6.

Bellucci, A., and K. J. Richards, 2006: Effects of NAO variability on the North Atlantic Ocean circulation. *Geophys. Res. Lett.*, **33**, L02612, https://doi.org/10.1029/2005GL024890.

——, S. Gualdi, E. Scoccimarro, and A. Navarra, 2008: NAO–ocean circulation interactions in a coupled general circulation model. *Climate Dyn.*, **31**, 759–777, https://doi.org/10.1007/s00382-008-0408-4.

Bower, A. S., M. S. Lozier, S. F. Gary, and C. W. Böning, 2009: Interior pathways of the North Atlantic meridional overturning circulation. *Nature*, **459**, 243–247, https://doi.org/10.1038/nature07979.

——, ——, and ——, 2011: Export of Labrador Sea water from the subpolar North Atlantic: A Lagrangian perspective. *Deep-Sea Res. II*, **58**, 1798–1818, https://doi.org/10.1016/j.dsr2.2010.10.060.

Brayshaw, D. J., B. Hoskins, and M. Blackburn, 2011: The basic ingredients of the North Atlantic storm track. Part II: Sea surface temperatures. *J. Atmos. Sci.*, **68**, 1784–1805, https://doi.org/10.1175/2011JAS3674.1.

Carton, J. A., G. A. Chepurin, and L. Chen, 2018: SODA3: A new ocean climate reanalysis. *J. Climate*, **31**, 6967–6983, https://doi.org/10.1175/JCLI-D-18-0149.1.

Chaudhuri, A. H., A. Gangopadhyay, and J. J. Bisagni, 2009: Interannual variability of Gulf Stream warm-core rings in response to the North Atlantic Oscillation. *Cont. Shelf Res.*, **29**, 856–869, https://doi.org/10.1016/j.csr.2009.01.008.

Cipollini, P., D. Cromwell, M. S. Jones, G. D. Quartly, and P. G. Challenor, 1997: Concurrent altimeter and infrared observations of Rossby wave propagation near 34°N in the northeast Atlantic. *Geophys. Res. Lett.*, **24**, 889–892, https://doi.org/10.1029/97GL00758.

——, ——, P. G. Challenor, and S. Raffaglio, 2001: Rossby waves detected in global ocean colour data. *Geophys. Res. Lett.*, **28**, 323–326, https://doi.org/10.1029/1999GL011231.

Csanady, G. T., and P. Hamilton, 1988: Circulation of slopewater. *Cont. Shelf Res.*, **8**, 565–624, https://doi.org/10.1016/0278-4343(88)90068-4.

de Coëtlogon, G., C. Frankignoul, M. Bentsen, C. Delon, H. Haak, S. Masina, and A. Pardaens, 2006: Gulf Stream variability in five oceanic general circulation models. *J. Phys. Oceanogr.*, **36**, 2119–2135, https://doi.org/10.1175/JPO2963.1.

Deser, C., M. A. Alexander, S.-P. Xie, and A. S. Phillips, 2010: Sea surface temperature variability: Patterns and mechanisms. *Annu. Rev. Mar. Sci.*, **2**, 115–143, https://doi.org/10.1146/annurev-marine-120408-151453.

Diabaté, S. T., D. Swingedouw, J. J.-M. Hirschi, A. Duchez, P. J. Leadbitter, I. D. Haigh, and G. D. McCarthy, 2021: Western boundary circulation and coastal sea-level variability in Northern Hemisphere oceans. *Ocean Sci.*, **17**, 1449–1471, https://doi.org/10.5194/os-17-1449-2021.

Duchon, C. E., 1979: Lanczos filtering in one and two dimensions. *J. Appl. Meteor.*, **18**, 1016–1022, https://doi.org/10.1175/1520-0450(1979)018<1016:LFIOAT>2.0.CO;2.

Ebisuzaki, W., 1997: A method to estimate the statistical significance of a correlation when the data are serially correlated. *J. Climate*, **10**, 2147–2153, https://doi.org/10.1175/1520-0442(1997)010<2147:AMTETS>2.0.CO;2.

Eden, C., and R. J. Greatbatch, 2003: A damped decadal oscillation in the North Atlantic climate system. *J. Climate*, **16**, 4043–4060, https://doi.org/10.1175/1520-0442(2003)016<4043:ADDOIT>2.0.CO;2.

Esselborn, S., and C. Eden, 2001: Sea surface height changes in the North Atlantic Ocean related to the North Atlantic Oscillation. *Geophys. Res. Lett.*, **28**, 3473–3476, https://doi.org/10.1029/2001GL012863.

Famooss Paolini, L., P. J. Athanasiadis, P. Ruggieri, and A. Bellucci, 2022: The atmospheric response to meridional shifts of the Gulf Stream SST front and its dependence on model resolution. *J. Climate*, **35**, 6007–6030, https://doi.org/10.1175/JCLI-D-21-0530.1.

Farge, M., 1992: Wavelet transforms and their applications to turbulence. *Annu. Rev. Fluid Mech.*, **24**, 395–458, https://doi.org/10.1146/annurev.fl.24.010192.002143.

Frankignoul, C., G. de Coëtlogon, T. M. Joyce, and S. Dong, 2001: Gulf Stream variability and ocean–atmosphere interactions. *J. Phys. Oceanogr.*, **31**, 3516–3529, https://doi.org/10.1175/1520-0485(2002)031<3516:GSVAOA>2.0.CO;2.

Fu, L.-L., and B. Qiu, 2002: Low-frequency variability of the North Pacific Ocean: The roles of boundary- and wind-driven baroclinic Rossby waves. *J. Geophys. Res.*, **107**, 3220, https://doi.org/10.1029/2001JC001131.

Gangopadhyay, A., P. Cornillon, and D. R. Watts, 1992: A test of the Parsons–Veronis hypothesis on the separation of the Gulf Stream. *J. Phys. Oceanogr.*, **22**, 1286–1301, https://doi.org/10.1175/1520-0485(1992)022<1286:ATOTPH>2.0.CO;2.

——, A. H. Chaudhuri, and A. H. Taylor, 2016: On the nature of temporal variability of the Gulf Stream path from 75° to 55°W. *Earth Interact.*, **20**, https://doi.org/10.1175/EI-D-15-0025.1.

Georgiou, S., S. L. Ypma, N. Brüggemann, J.-M. Sayol, J. D. Pietrzak, and C. A. Katsman, 2020: Pathways of the water masses exiting the Labrador Sea: The importance of boundary–interior exchanges. *Ocean Modell.*, **150**, 101623, https://doi.org/10.1016/j.ocemod.2020.101623.

Getzlaff, J., C. W. Böning, C. Eden, and A. Biastoch, 2005: Signal propagation related to the North Atlantic overturning. *Geophys. Res. Lett.*, **32**, L09602, https://doi.org/10.1029/2004GL021002.

Grinsted, A., J. C. Moore, and S. Jevrejeva, 2004: Application of the cross wavelet transform and wavelet coherence to geophysical time series. *Nonlinear Processes Geophys.*, **11**, 561–566, https://doi.org/10.5194/npg-11-561-2004.

Häkkinen, S., P. B. Rhines, and D. L. Worthen, 2011: Atmospheric blocking and Atlantic multidecadal ocean variability. *Science*, **334**, 655–659, https://doi.org/10.1126/science.1205683.

Hameed, S., and S. Piontkovski, 2004: The dominant influence of the Icelandic low on the position of the Gulf Stream northwall. *Geophys. Res. Lett.*, **31**, L09303, https://doi.org/10.1029/2004GL019561.

——, C. L. P. Wolfe, and L. Chi, 2018: Impact of the Atlantic meridional mode on Gulf Stream north wall position. *J. Climate*, **31**, 8875–8894, https://doi.org/10.1175/JCLI-D-18-0098.1.

Hersbach, H., and Coauthors, 2020: The ERA5 global reanalysis. *Quart. J. Roy. Meteor. Soc.*, **146**, 1999–2049, https://doi.org/10.1002/qj.3803.

Hogg, N. G., 1992: On the transport of the Gulf Stream between Cape Hatteras and the grand banks. *Deep-Sea Res.*, **39A**, 1231–1246, https://doi.org/10.1016/0198-0149(92)90066-3.

Holliday, N. P., and Coauthors, 2020: Ocean circulation causes the largest freshening event for 120 years in eastern subpolar North Atlantic. *Nat. Commun.*, **11**, 585, https://doi.org/10.1038/s41467-020-14474-y.

Hovmöller, E., 1949: The trough-and-ridge diagram. *Tellus*, **1** (2), 62–66, https://doi.org/10.3402/tellusa.v1i2.8498.

Hudgins, L., C. A. Friehe, and M. E. Mayer, 1993: Wavelet transforms and atmospheric turbulence. *Phys. Rev. Lett.*, **71**, 3279–3282, https://doi.org/10.1103/PhysRevLett.71.3279.

Hurrell, J. W., 1995: Decadal trends in the North Atlantic Oscillation: Regional temperatures and precipitation. *Science*, **269**, 676–679, https://doi.org/10.1126/science.269.5224.

——, Y. Kushnir, G. Ottersen, and M. Visbeck, Eds., 2003: *The North Atlantic Oscillation: Climatic Significance and Environmental Impact*. *Geophys. Monogr.*, Vol. 134, Amer. Geophys. Union, https://doi.org/10.1029/GM134.

Johnson, H. L., and D. P. Marshall, 2002: A theory for the surface Atlantic response to thermohaline variability. *J. Phys. Oceanogr.*, **32**, 1121–1132, https://doi.org/10.1175/1520-0485(2002)032<1121:ATFTSA>2.0.CO;2.

Joyce, T. M., and R. Zhang, 2010: On the path of the Gulf Stream and the Atlantic meridional overturning circulation. *J. Climate*, **23**, 3146–3154, https://doi.org/10.1175/2010JCLI3310.1.

——, C. Deser, and M. A. Spall, 2000: The relation between decadal variability of subtropical mode water and the North Atlantic Oscillation. *J. Climate*, **13**, 2550–2569, https://doi.org/10.1175/1520-0442(2000)013<2550:TRBDVO>2.0.CO;2.

——, Y.-O. Kwon, and L. Yu, 2009: On the relationship between synoptic wintertime atmospheric variability and path shifts in the Gulf Stream and the Kuroshio Extension. *J. Climate*, **22**, 3177–3192, https://doi.org/10.1175/2008JCLI2690.1.

——, ——, H. Seo, and C. C. Ummenhofer, 2019: Meridional Gulf Stream shifts can influence wintertime variability in the North Atlantic storm track and Greenland blocking. *Geophys. Res. Lett.*, **46**, 1702–1708, https://doi.org/10.1029/2018GL081087.

Kallberg, P., P. Berrisford, B. J. Hoskins, A. Simmons, S. Uppala, S. Lamy-Thepaut, and R. Hine, 2005: ERA-40 Atlas. ERA-40 Project Rep. Series 19, 199 pp.

Kenigson, J. S., W. Han, B. Rajagopalan, Yanto, and M. Jasinski, 2018: Decadal shift of NAO-linked interannual sea level variability along the U.S. northeast coast. *J. Climate*, **31**, 4981–4989, https://doi.org/10.1175/JCLI-D-17-0403.1.

Kohyama, T., Y. Yamagami, H. Miura, S. Kido, H. Tatebe, and M. Watanabe, 2021: The Gulf Stream and Kuroshio Current are synchronized. *Science*, **374**, 341–346, https://doi.org/10.1126/science.abh3295.

Kowalski, P., 2022: On the contribution of Rossby waves driven by surface buoyancy fluxes to low-frequency North Atlantic steric sea surface height variations. *Atmos. Oceanic Sci. Lett.*, **15**, 100153, https://doi.org/10.1016/j.aosl.2022.100153.

Kwon, Y.-O., and T. M. Joyce, 2013: Northern Hemisphere winter atmospheric transient eddy heat fluxes and the Gulf Stream and Kuroshio–Oyashio Extension variability. *J. Climate*, **26**, 9839–9859, https://doi.org/10.1175/JCLI-D-12-00647.1.

——, M. A. Alexander, N. A. Bond, C. Frankignoul, H. Nakamura, B. Qiu, and L. A. Thompson, 2010: Role of the Gulf Stream and Kuroshio–Oyashio systems in large-scale atmosphere–ocean interaction: A review. *J. Climate*, **23**, 3249–3281, https://doi.org/10.1175/2010JCLI3343.1.

Lillibridge, J. L., III, and A. J. Mariano, 2013: A statistical analysis of Gulf Stream variability from 18+ years of altimetry data. *Deep-Sea Res. II*, **85**, 127–146, https://doi.org/10.1016/j.dsr2.2012.07.034.

Maraun, D., and J. Kurths, 2004: Cross wavelet analysis: Significance testing and pitfalls. *Nonlinear Processes Geophys.*, **11**, 505–514, https://doi.org/10.5194/npg-11-505-2004.

Marshall, J., H. Johnson, and J. Goodman, 2001: A study of the interaction of the North Atlantic Oscillation with ocean circulation. *J. Climate*, **14**, 1399–1421, https://doi.org/10.1175/1520-0442(2001)014<1399:ASOTIO>2.0.CO;2.

Molinari, R. L., R. A. Fine, W. D. Wilson, R. G. Curry, J. Abell, and M. S. McCartney, 1998: The arrival of recently formed Labrador Sea water in the deep western boundary current at 26.5°N. *Geophys. Res. Lett.*, **25**, 2249–2252, https://doi.org/10.1029/98GL01853.

Nakamura, M., and S. Yamane, 2009: Dominant anomaly patterns in the near-surface baroclinicity and accompanying anomalies in the atmosphere and oceans. Part I: North Atlantic Basin. *J. Climate*, **22**, 880–904, https://doi.org/10.1175/2008JCLI2297.1.

New, A. L., D. A. Smeed, A. Czaja, A. T. Blaker, J. V. Mecking, J. P. Mathews, and A. Sanchez-Franks, 2021: Labrador Slope Water connects the subarctic with the Gulf Stream. *Environ. Res. Lett.*, **16**, 084019, https://doi.org/10.1088/1748-9326/ac1293.

Nigam, S., A. Ruiz-Barradas, and L. Chafik, 2018: Gulf Stream excursions and sectional detachments generate the decadal pulses in the Atlantic multidecadal oscillation. *J. Climate*, **31**, 2853–2870, https://doi.org/10.1175/JCLI-D-17-0010.1.

Omrani, N.-E., F. Ogawa, H. Nakamura, N. Keenlyside, S. W. Lubis, and K. Matthes, 2019: Key role of the ocean western boundary currents in shaping the Northern Hemisphere climate. *Sci. Rep.*, **9**, 3014, https://doi.org/10.1038/s41598-019-39392-y.

——, N. Keenlyside, K. Matthes, L. Boljka, D. Zanchettin, J. H. Jungclaus, and S. W. Lubis, 2022: Coupled stratosphere-troposphere-Atlantic multidecadal oscillation and its importance for near-future climate projection. *npj Climate Atmos. Sci.*, **5**, 59, https://doi.org/10.1038/s41612-022-00275-1.

O'Reilly, C. H., S. Minobe, and A. Kuwano-Yoshida, 2016: The influence of the Gulf Stream on wintertime European blocking. *Climate Dyn.*, **47**, 1545–1567, https://doi.org/10.1007/s00382-015-2919-0.

Osychny, V., and P. Cornillon, 2004: Properties of Rossby waves in the North Atlantic estimated from satellite data. *J. Phys. Oceanogr.*, **34**, 61–76, https://doi.org/10.1175/1520-0485(2004)034<0061:PORWIT>2.0.CO;2.

Peña-Molino, B., and T. M. Joyce, 2008: Variability in the slope water and its relation to the Gulf Stream path. *Geophys. Res. Lett.*, **35**, L03606, https://doi.org/10.1029/2007GL032183.

——, ——, and J. M. Toole, 2011: Recent changes in the Labrador Sea Water within the deep western boundary current southeast of Cape Cod. *Deep-Sea Res. I*, **58**, 1019–1030, https://doi.org/10.1016/j.dsr.2011.07.006.

Percival, D. P., 1995: On estimation of the wavelet variance. *Biometrika*, **82**, 619–631, https://doi.org/10.1093/biomet/82.3.619.

Pérez-Hernández, M. D., and T. M. Joyce, 2014: Two modes of Gulf Stream variability revealed in the last two decades of satellite altimeter data. *J. Phys. Oceanogr.*, **44**, 149–163, https://doi.org/10.1175/JPO-D-13-0136.1.

Peterson, I., B. Greenan, D. Gilbert, and D. Hebert, 2017: Variability and wind forcing of ocean temperature and thermal fronts in the slope water region of the northwest Atlantic. *J. Geophys. Res. Oceans*, **122**, 7325–7343, https://doi.org/10.1002/2017JC012788.

Pickart, R. S., 1992: Water mass components of the North Atlantic deep western boundary current. *Deep-Sea Res.*, **39A**, 1553–1572, https://doi.org/10.1016/0198-0149(92)90047-W.

——, and W. M. Smethie Jr., 1993: How does the deep western boundary current cross the Gulf Stream? *J. Phys. Oceanogr.*, **23**, 2602–2616, https://doi.org/10.1175/1520-0485(1993)023<2602:HDTDWB>2.0.CO;2.

Reintges, A., M. Latif, and W. Park, 2017: Sub-decadal North Atlantic Oscillation variability in observations and the Kiel Climate Model. *Climate Dyn.*, **48**, 3475–3487, https://doi.org/10.1007/s00382-016-3279-0.

Rossby, T., 1999: On gyre interactions. *Deep-Sea Res. II*, **46**, 139–164, https://doi.org/10.1016/S0967-0645(98)00095-2.

——, and R. L. Benway, 2000: Slow variations in mean path of the Gulf Stream east of Cape Hatteras. *Geophys. Res. Lett.*, **27**, 117–120, https://doi.org/10.1029/1999GL002356.

——, C. N. Flagg, and K. Donohue, 2005: Interannual variations in upper-ocean transport by the Gulf Stream and adjacent waters between New Jersey and Bermuda. *J. Mar. Res.*, **63**, 203–226, https://elischolar.library.yale.edu/journal_of_marine_research/77/.

Sanchez-Franks, A., and R. Zhang, 2015: Impact of the Atlantic meridional overturning circulation on the decadal variability of the Gulf Stream path and regional chlorophyll and nutrient concentrations. *Geophys. Res. Lett.*, **42**, 9889–9897, https://doi.org/10.1002/2015GL066262.

——, S. Hameed, and R. E. Wilson, 2016: The Icelandic low as a predictor of the Gulf Stream north wall position. *J. Phys. Oceanogr.*, **46**, 817–826, https://doi.org/10.1175/JPO-D-14-0244.1.

Sasaki, Y. N., and N. Schneider, 2011: Interannual to decadal Gulf Stream variability in an eddy-resolving ocean model. *Ocean Modell.*, **39**, 209–219, https://doi.org/10.1016/j.ocemod.2011.04.004.

Sato, K., J. Inoue, and M. Watanabe, 2014: Influence of the Gulf Stream on the Barents Sea ice retreat and Eurasian coldness during early winter. *Environ. Res. Lett.*, **9**, 084009, https://doi.org/10.1088/1748-9326/9/8/084009.

Smethie, W. M., Jr., 1993: Tracing the thermohaline circulation in the western North Atlantic using chlorofluorocarbons. *Prog. Oceanogr.*, **31**, 51–99, https://doi.org/10.1016/0079-6611(93)90023-7.

Spall, M. A., 1996: Dynamics of the Gulf Stream/deep western boundary current crossover. Part I: Entrainment and recirculation. *J. Phys. Oceanogr.*, **26**, 2152–2168, https://doi.org/10.1175/1520-0485(1996)026<2152:DOTGSW>2.0.CO;2.

Stommel, H., 1958: The abyssal circulation. *Deep-Sea Res.*, **5**, 80–82, https://doi.org/10.1016/S0146-6291(58)80014-4.

Sturges, W., and B. G. Hong, 1995: Wind forcing of the Atlantic thermocline along 32°N at low frequencies. *J. Phys. Oceanogr.*, **25**, 1706–1715, https://doi.org/10.1175/1520-0485(1995)025<1706:WFOTAT>2.0.CO;2.

——, ——, and A. J. Clarke, 1998: Decadal wind forcing of the North Atlantic subtropical gyre. *J. Phys. Oceanogr.*, **28**, 659–668, https://doi.org/10.1175/1520-0485(1998)028<0659:DWFOTN>2.0.CO;2.

Talley, L. D., and M. S. McCartney, 1982: Distribution and circulation of Labrador Sea Water. *J. Phys. Oceanogr.*, **12**, 1189–1205, https://doi.org/10.1175/1520-0485(1982)012<1189:DACOLS>2.0.CO;2.

Taylor, A. H., and J. A. Stephens, 1998: The North Atlantic Oscillation and the latitude of the Gulf Stream. *Tellus*, **50A**, 134–142, https://doi.org/10.3402/tellusa.v50i1.14517.

——, and A. Gangopadhyay, 2001: A simple model of interannual displacements of the Gulf Stream. *J. Geophys. Res.*, **106**, 13 849–13 860, https://doi.org/10.1029/1999JC000147.

——, M. B. Jordan, and J. A. Stephens, 1998: Gulf Stream shifts following ENSO events. *Nature*, **393**, 638, https://doi.org/10.1038/31380.

Torrence, C., and G. P. Compo, 1998: A practical guide to wavelet analysis. *Bull. Amer. Meteor. Soc.*, **79**, 61–78, https://doi.org/10.1175/1520-0477(1998)079<0061:APGTWA>2.0.CO;2.

——, and P. J. Webster, 1999: Interdecadal changes in the ENSO–monsoon system. *J. Climate*, **12**, 2679–2690, https://doi.org/10.1175/1520-0442(1999)012<2679:ICITEM>2.0.CO;2.

Veronis, G., 1973: Model of world ocean circulation: I. Wind-driven, two layer. *J. Mar. Res.*, **31**, 228–288.

Visbeck, M., H. Cullen, G. Krahmann, and N. Naik, 1998: An ocean model's response to North Atlantic Oscillation-like wind forcing. *Geophys. Res. Lett.*, **25**, 4521–4524, https://doi.org/10.1029/1998GL900162.

——, E. P. Chassignet, R. G. Curry, T. L. Delworth, R. R. Dickson, and G. Krahmann, 2003: The Ocean's response to North Atlantic Oscillation variability. *The North Atlantic Oscillation: Climatic Significance and Environmental Impact*, *Geophys. Monogr.*, Vol. 134, Amer. Geophys. Union, 113–145, https://doi.org/10.1029/134GM06.

Watelet, S., J.-M. Beckers, and A. Barth, 2017: Reconstruction of the Gulf Stream from 1940 to the present and correlation with the North Atlantic Oscillation. *J. Phys. Oceanogr.*, **47**, 2741–2754, https://doi.org/10.1175/JPO-D-17-0064.1.

——, ——, J.-M. Molines, and C. Troupin, 2020: Properties of baroclinic Rossby waves in the North Atlantic from eddy-resolving simulations of ocean circulation. *Ocean Sci. Discuss.*, https://doi.org/10.5194/os-2020-79, preprint.

Wolfe, C. L. P., S. Hameed, and L. Chi, 2019: On the drivers of decadal variability of the Gulf Stream north wall. *J. Climate*, **32**, 1235–1249, https://doi.org/10.1175/JCLI-D-18-0212.1.

Worthington, L. V., 1976: *On the North Atlantic Circulation*. The Johns Hopkins University Press, 110 pp.

Zhang, J., K. A. Kelly, and L. Thompson, 2016: The role of heating, winds, and topography on sea level changes in the North Atlantic. *J. Geophys. Res. Oceans*, **121**, 2887–2900, https://doi.org/10.1002/2015JC011492.

Zhang, R., 2010: Latitudinal dependence of Atlantic meridional overturning circulation (AMOC) variations. *Geophys. Res. Lett.*, **37**, L16703, https://doi.org/10.1029/2010GL044474.

——, and G. K. Vallis, 2006: Impact of great salinity anomalies on the low-frequency variability of the North Atlantic climate. *J. Climate*, **19**, 470–482, https://doi.org/10.1175/JCLI3623.1.

——, and ——, 2007: The role of bottom vortex stretching on the path of the North Atlantic western boundary current and on the northern recirculation gyre. *J. Phys. Oceanogr.*, **37**, 2053–2080, https://doi.org/10.1175/JPO3102.1.

Zuo, H., M. A. Balmaseda, S. Tietsche, K. Mogensen, and M. Mayer, 2019: The ECMWF operational ensemble reanalysis–analysis system for ocean and sea ice: A description of the system and assessment. *Ocean Sci.*, **15**, 779–808, https://doi.org/10.5194/os-15-779-2019.